[American Journal of Science, Vol. 302, March, 2002, P. 191–226]

SHRIMP U–Pb ZIRCON AGES OF THE FUPING COMPLEX: IMPLICATIONS FOR LATE ARCHEAN TO PALEOPROTEROZOIC ACCRETION AND ASSEMBLY OF THE NORTH CHINA CRATON

GUOCHUN ZHAO*, SIMON A. WILDE**,
PETER A. CAWOOD**, and MIN SUN***

ABSTRACT. **The Fuping Complex is situated in the central part of the North China Craton and consists of four major lithological assemblages: Fuping tonalitic–trondhjemitic–granodioritic gneisses, Longquanguan augen gneisses, Wanzi supracrustal assemblage and Nanying granitic gneisses. SHRIMP U–Pb geochronology combined with U–Th and cathodoluminescence (CL) imaging of zircon enables resolution of magmatic and metamorphic events that can be directed towards understanding the late Archean to Paleoproterozoic history of the Fuping Complex. CL images reveal the coexistence of magmatic and metamorphic zircons in nearly all rock types of the Fuping Complex. The metamorphic zircons occur as either single grains or overgrowth (or recrystallization) rims surrounding and truncating oscillatory-zoned magmatic zircon cores, and are all characterized by nebulous zoning or being structureless, with extremely high luminescence and very low Th contents. These features make them distinct from magmatic zircons that are characterized by concentric oscillatory zoning, comparatively low luminescence and high Th and U contents.**

SHRIMP U–Pb analyses on magmatic zircons reveal that the tonalitic, trondhjemitic and granodioritic plutons of the Fuping gneisses were emplaced at 2523 ± 14 Ma, 2499 ± 10 Ma and 2486 ± 8 Ma, respectively; whereas the monzogranitic and granitic plutons of the Longquanguan augen gneisses were intruded, respectively, at 2510 ± 22 Ma and 2507 ± 11 Ma. Prismatic and oscillatory-zoned zircons dominate in the pelitic rocks of the Wanzi supracrustal assemblage and are interpreted as detritus from igneous source rocks. The concordant and discordant U–Pb ages of 2502 ± 5 Ma and 2507 ± 14 Ma obtained from two pelitic rock samples indicate these rocks must have been deposited no earlier than ~2507 Ma ago. In addition, a zoned zircon grain in one pelitic rock sample has a near concordant age of 2109 ± 5 (1σ) Ma, which may provide a maximum depositional age for the Wanzi supracrustal rocks. SHRIMP results also reveal that granitic magmatism assigned to the Nanying granitic gneisses occurred over a protracted interval from ~2077 ± 13 Ma to ~2024 ± 21 Ma. The nebulously-zoned zircon grains and overgrowth/recrystallization zircon rims from different rocks yielded similar concordant $^{207}Pb/^{206}Pb$ ages in the range 1875 to 1802 Ma, interpreted as approximating the age of regional metamorphism of the Fuping Complex.

Timing of primary zircon crystallization and regional metamorphism of the Fuping Complex is in general agreement with recent U–Pb zircon ion probe results for the Wutai and Hengshan Complexes that bound the Fuping Complex to the northwest. These areas are characterized by the emplacement of major granitoid bodies at around 2.50 Ga to 2.48 Ga ago, deposition of supracrustal rocks in the Paleoproterozoic, intrusion of Paleoproterozoic granitic bodies at 2.1 to 2.0 Ga, and regional metamorphism at 1.875 to 1.802 Ga. These data indicate that the Fuping and Hengshan Complexes do not represent an older crystalline basement to the Wutai Complex, as suggested in previous tectonic models but, together with the Wutai Complex, represent elements of a single late Archean to Paleoproterozoic magmatic arc system that has been subsequently tectonically disrupted and juxtaposed during the collision of the

*Tectonics Special Research Centre, School of Applied Geology, Curtin University of Technology, GPO Box U1987, Perth, 6001 Australia. Present address: Department of Earth Sciences, University of Hong Kong, Pokfulam Road, Hong Kong, China

**Tectonics Special Research Centre, School of Applied Geology, Curtin University of Technology, GPO Box U1987, Perth, 6001 Australia

***Department of Earth Sciences, University of Hong Kong, Pokfulam Road, Hong Kong, China

eastern and western North China blocks at ~1.85 Ga, which resulted in the final assembly of the North China Craton.

INTRODUCTION

The North China Craton is the largest and oldest known cratonic block in China. Although much is now known of the geology of the craton, including the economic mineral occurrences, its tectonic subdivision and evolution has not been well constrained. Traditionally, the North China Craton has been considered to be composed of relatively uniform Archean to Paleoproterozoic basement, and its tectonic history was explained using a pre-plate tectonic geosynclinal model (Huang, 1977). However, recent geological data have revealed significant differences between the central part and eastern/western part of the craton (Wu and Zhong, 1998; Zhao and others, 2001a; Wu and others, 2000). For example, fragments of ancient oceanic crust, melanges, HP granulites/amphibolites and retrograded eclogites have been found only in the central part of the craton (Bai, 1986; Li and others, 1990; Zhai, Guo, and Yan, 1992; Zhai and others, 1995; Wang and others, 1996; Bai and Dai, 1998; Guo and others, 1993, 1998, 1999, 2001; Guo and Zhai, 2001; Zhao and others, 2001b), whereas the eastern and western parts of the craton are dominated by Archean tonalitic–trondhjemitic–granodioritic gneiss complexes surrounded by minor supracrustal rocks (Jahn and Zhang, 1984; Ma and others, 1987; He and Ye, 1998; Zhao and others, 1998). In addition, petrographic and thermobarometric data have revealed that metamorphic rocks in the central part of the craton differ in metamorphic P–T evolution from those in the eastern and western parts of the craton (Zhao and others, 1998, 1999a, b). The former underwent metamorphism characterized by clockwise P–T paths involving isothermal decompression, reflecting continental collisional environments (Zhao and others, 2000a, b), whereas the latter experienced metamorphism at ~2.5 Ga, with anticlockwise P–T paths involving isobaric cooling, reflecting underplating and intrusion of mantle-derived magmas (Zhao and others, 1998). The discovery of these differences led to a new three-fold division of the North China Craton into the Eastern and Western Blocks, separated by a 100–300 km wide crustal boundary zone, called the Central Zone (Zhao and others, 2001a). Considering the spatial and time relationships between the Central Zone and Eastern and Western Blocks, Zhao (2001) proposed that the Central Zone represents a Paleoproterozoic collisional orogen along which the Eastern and Western blocks amalgamated to form the North China Craton. A coherent outline of tectonic processes involved in the amalgamation of the craton has recently emerged and there is also much increased knowledge concerning the pre-amalgamation histories of the Eastern and Western Blocks that were subsequently incorporated into the North China Craton (Zhao and others, 1998; Zhao and others, 1999b; Zhao and others, 2000b; Wu and Zhong, 1998; Wu and others, 2000b). However, controversy remains with the timing of the amalgamation of the Eastern and Western Blocks, with some workers believing that the amalgamation occurred at ~2.5 Ga (Li and others, 2000; Zhai, Bian, and Zhao, 2000). To resolve this controversy, it is essential to carry out extensive, high-resolution, geochronological investigations on various lithologies in the Central Zone.

The Fuping Complex, one of the largest metamorphic complexes in the Central Zone, is regarded as the most promising area for investigating the timing of magmatic and tectonometamorphic events occurring in the Central Zone because of its representative lithological assemblages and excellent exposures. Also, the complex, in conjunction with the adjoining Wutai and Hengshan Complexes, has long been considered to represent a classic Precambrian orogenic belt in the North China Craton (Ma and others, 1987; Tian, 1991; Bai and others, 1992; Wang and others, 1996). Of particular significance is the presence of a low-grade granite–greenstone terrane (Wutai Complex) intervening between two high-grade gneiss complexes (Hengshan and Fuping

Complexes). Two contrasting tectonic models have been proposed for the evolution of the orogenic belt. One model suggests that the Fuping and Hengshan Complexes developed as a single continental block that underwent late Archean rifting associated with formation of the Wutai greenstones and closed upon itself in the Paleoproterozoic (Tian, 1991; Yuan and Zhang, 1993). The other model proposes that the orogenic belt is a late Archean continent–arc–continent collision system, in which the Fuping and Hengshan Complexes represent two exotic Archean continental blocks, and the Wutai granite-greenstone represents an intervening island arc (Bai, 1986; Li and others, 1990; Bai and others, 1992; Wang and others, 1996). Although these models propose different tectonic settings and processes for the evolution of the orogenic belt, they both assume that the high-grade Fuping and Hengshan Complexes are older in their protolith and metamorphic age than the low-grade Wutai Complex. This assumption is based on conventional multigrain U–Pb zircon geochronology (Liu and others, 1985; Bai, 1986; Wu and others, 1989), but has not been tested using the Sensitive High Resolution Ion Micro Probe (SHRIMP). Published U–Pb ages, determined by the isotope dilution method, gave intercept ages, but the inconsistent upper and lower intersection ages and large uncertainties suggest that these multigrain data-points most likely represent a mixture of zircons with different ages. For this reason, most multigrain zircon ages for the Fuping, Wutai and Hengshan Complexes should be viewed with caution.

The purpose of this communication is to present new SHRIMP U–Pb ages for the complexly zoned zircons in the rocks of the Fuping Complex. To aid our interpretations, we utilize CL images of single zircon grains, which are helpful for resolving single-crystal domains of magmatic, metamorphic or detrital origin. The ages determined from this study will enable a re-evaluation of the above tectonic models and place rigorous constraints on the late Archean to Paleoproterozoic accretion and assembly of the North China Craton.

REGIONAL SETTING

North China Craton.—The South China, Tarim, and North China Cratons are the three major cratonic blocks in China (fig. 1). The South China Craton consists of the Yangtze and Cathaysia Blocks that amalgamated along the Jiangshan–Shaoxing suture (JSS) during the ~1.0–0.85 Ga Jinning orogeny (fig. 1; Shui, 1987; Zhao and Cawood, 1999). The Tarim Craton consists of late Archean to Paleoproterozoic gneisses and schists but its tectonic evolution is not well constrained. The North China Craton, a general term used to refer to the Chinese part of the Sino–Korean Craton, is bounded on the west and north by the early Paleozoic Qilianshan (QLS) and the late Paleozoic Tianshan–Inner Mongolia–Daxinganling (TIMD) orogens, respectively, and separated from the Yangtze Block by the Qinling–Dabie–Su–Lu (QDSL) ultrahigh-pressure belt of Mesozoic age (Rowley and others, 1997). The North China Craton consists of Early Archean to Paleoproterozoic crystalline rocks overlain unconformably by Mesoproterozoic to Cenozoic sedimentary strata. Early Archean crystalline rocks, ranging in age from 3.85 to 3.4 Ga, have been reported from the Eastern Hebei and Anshan–Benxi Complexes (Liu and others, 1992; Song and others, 1996) and are composed predominantly of mafic amphibolites, granitic gneisses and metamorphosed supracrustal rocks (Huang and others, 1986; Jahn and others, 1987; Liu and others, 1992; Song and others, 1996). The mid-Archean crystalline rocks consist mainly of mafic granulites, amphibolites and greenschists, with minor pelitic and granitic gneisses that range in age from 3.4 to 2.9 Ga (Huang and others, 1986; Jahn and others, 1987; Kröner and others, 1988; Wu and others, 1991). Late Archean crystalline rocks are widespread over the whole of the North China Craton, making up 85 percent of the total exposure of the basement. These rocks consist of 2.6 to 2.5 Ga tonalitic, trondhjemitic and granodioritic gneisses, ~2.5 Ga syntectonic granites and a variety of supracrustal rocks

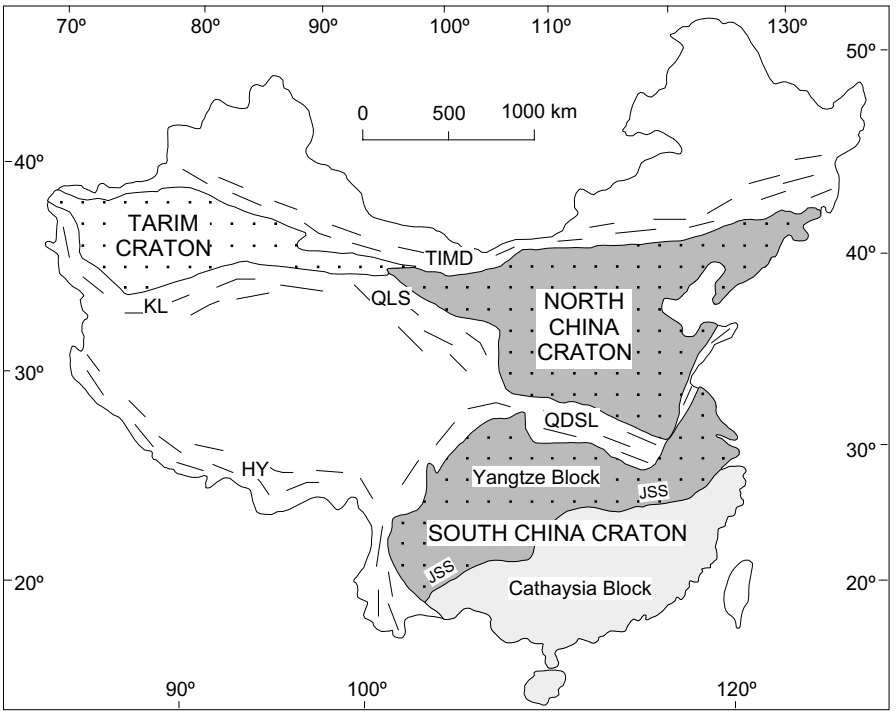

Fig. 1. Schematic tectonic map of China showing the major Precambrian blocks and Late Neoproterozoic and Paleozoic fold belts. HY–Himalaya fold belt; KL–Kunlun fold belt; JSS–Jiangshan–Shaoxing suture; QDSL–Qinlin–Dabie–Su–Lu fold belt; QLS–Qilianshan fold belt; TIMD–Tianshan–Inner Mongolia–Daxinganling fold belt.

that underwent greenschist to granulite facies regional metamorphism and polyphase deformation about 2.5 billion years ago (Jahn and Zhang, 1984; Liu and others, 1985; Shen and others, 1987; Kröner and others, 1998). Crystalline rocks of Paleoproterozoic age are subdivided into pelitic gneiss-dominated supracrustal formations, felsic volcanics and granitoids rocks. In both the western and eastern parts of the craton, the Paleoproterozoic crystalline rocks unconformably overlie the late Archean rocks, whereas the crystalline rocks in the central part of the craton range in age from late Archean to Paleoproterozoic. The main deformation and metamorphism of the Paleoproterozoic crystalline rocks occurred during the Lüliang Orogeny about 1.8 billion years ago (Tian, 1991; Bai and Dai, 1998; He and Ye, 1998).

Fuping Complex.—The Fuping–Wutai–Hengshan region lies in the central part of the North China Craton and consists of three distinct tectonic complexes: the upper amphibolite to granulite facies Fuping and Hengshan Complexes in the southeast and northwest, respectively, separated by the greenschist to lower amphibolite facies Wutai Complex (fig. 2, inset). The Wutai Complex is a typical granite-greenstone belt (Bai, 1986; Tian, 1991). The Fuping Complex was previously considered to be unconformably overlain by the Wutai Complex along the "Tiebao unconformity" (Bai, 1986; Wu and others, 1989; Tian, 1991), but recent research has revealed that the so-called "Tiebao unconformity" is a regional-scale ductile shear zone, named the Longquanguan Ductile Shear Zone by Li and Qian (1991).

Based on lithological, structural, and geochemical characteristics, the Fuping Complex can be further divided into four distinct lithotectonic units, herein called the

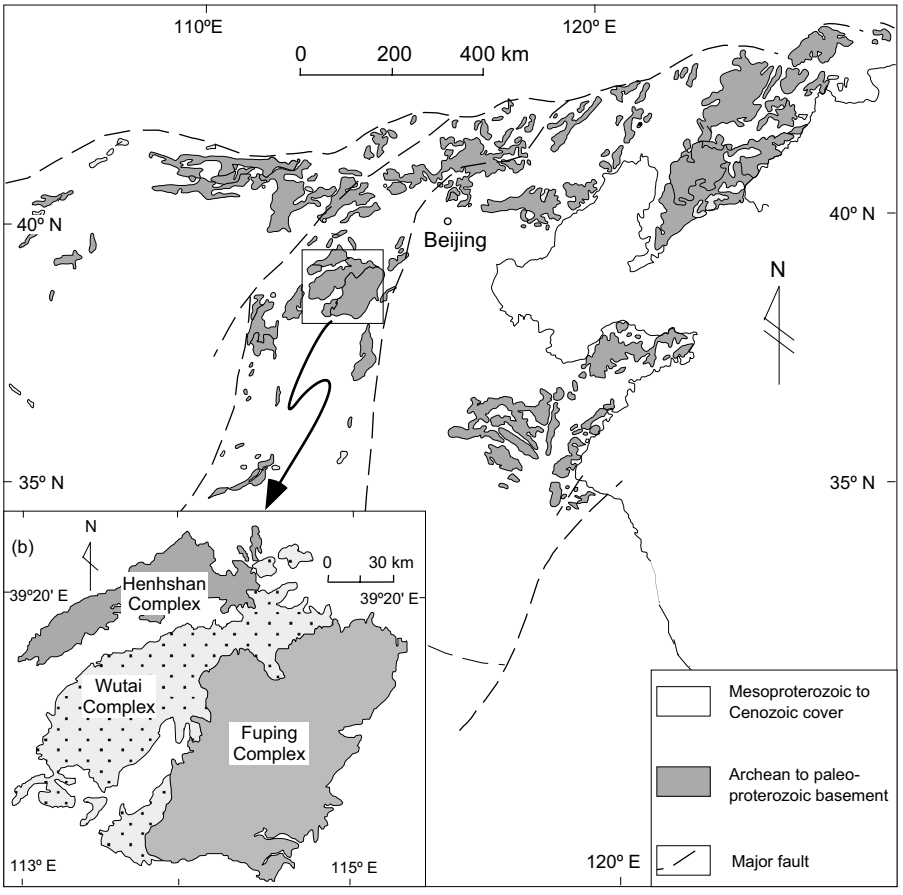

Fig. 2. Distribution of Early Precambrian rocks in the North China craton (revised after Zhao and others, 2001a). Inset: spatial relationship of the Fuping, Wutai and Hengshan Complexes.

Fuping gneisses, Longquanguan augen gneisses, Wanzi supracrustal assemblage, and Nanying granitic gneisses (fig. 3; Liu and Liang, 1997; Liu and others, 2000; Zhao and others, 2000a). The Fuping gneisses make up ~60 percent of the complex and consist of medium-grained tonalitic, trondhjemitic and granodioritic gneisses enclosing mafic granulites, amphibolites and hornblende gneisses that have undergone a complex history of upper amphibolite to granulite facies metamorphism and intense polyphase deformation. Petrological and geochemical data suggest that the Fuping gneisses were derived from the partial melting of mantle-derived basaltic rocks (Wang, Li, and Liu, 1991). The Fuping gneisses are interpreted to be in tectonic contact with the Wanzi supracrustal assemblage.

The Longquanguan augen gneisses, previously called the Longquanguan Group (Wu and others, 1989), are mainly exposed along the Longquanguan–Yulinping and Ciyu–Xinzhuang ductile shear zones (fig. 3) and composed predominantly of coarse-grained granodioritic and monzogranitic gneisses and mylonitized granitic pegmatites containing K-feldspar phenocrysts, most of which have been intensely deformed to form augen. Enclosed in the Longquanguan augen gneisses are amphibolite and hornblende gneiss enclaves, similar to those in the Fuping gneisses. Along the Ciyu–Xinzhuang ductile shear zone, a gradual transition from weakly-mylonitized to

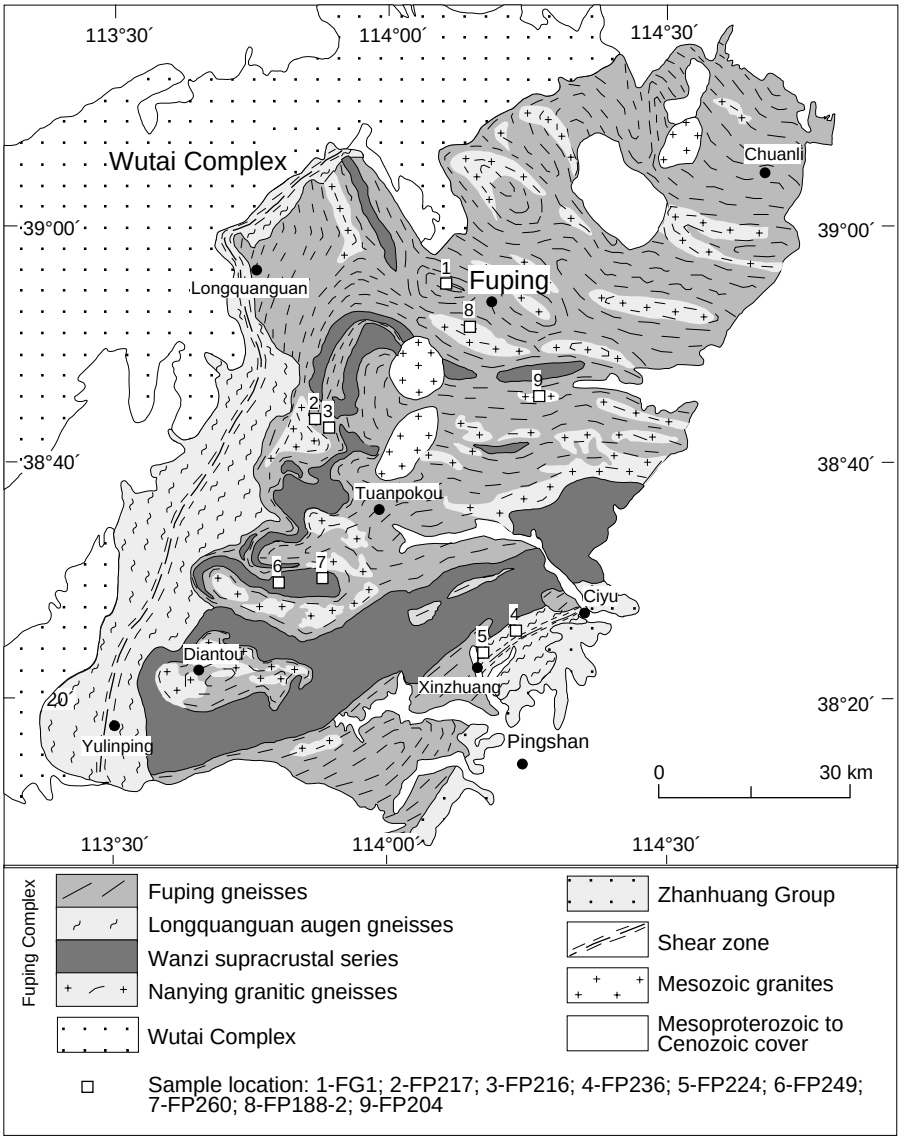

Fig. 3. Geological map of the Fuping Complex (revised after Zhao and others, 2000a).

intensely-mylonitized granodioritic and monzogranitic gneisses has been observed. The Longquanguan augen gneisses show a tectonic contact with the Wanzi supracrustal assemblage, but have a gradual transitional relationship with the Fuping gneisses. They may represent reworking of the Fuping gneisses (Wu and others, 1989; Li and Qian, 1991).

The Wanzi supracrustal assemblage forms a 100 km long, northeast–southwest trending belt in the southern part of the complex (15 km wide) that swings northward to the central part of the complex, where it is extensively folded (fig. 3). The supracrustal rocks are metamorphosed to amphibolite facies and comprise felsic and pelitic gneisses, pelitic schists, calc-silicates, pure and impure marbles and amphibo-

lites (Liu, 1997; Liu and Liang, 1997; Tang and Liu, 1997). Also associated with the supracrustal rocks are some small sillimanite-bearing granites, which are considered to represent S-type granites derived from partial melting of pelitic gneisses and felsic paragneisses, respectively (Wu and others, 1989; Liu, Liang, and Hua, 1999).

The Nanying granitic gneisses only occur within the Fuping gneisses and are dominated by medium- to fine-grained, weakly-foliated, magnetite-bearing monzogranitic gneisses, with minor granodioritic gneisses (fig. 3; Liu, 1997). In addition to compositional differences, the Nanying gneisses are more massive in structure and homogenous in composition than the Fuping gneisses. In the field where contact relations are preserved, the Nanying granitic gneisses are clearly intrusive into the Fuping gneisses, but their relatively weak foliation is consistent and parallel to the strong, penetrative, foliation of the Fuping gneisses, suggesting that they underwent the same deformational event that resulted in the development of the regional foliation of the Fuping Complex.

PREVIOUS GEOCHRONOLOGY

The age of the rocks and metamorphic events in the Fuping Complex have been poorly constrained until recently. Existing dates are based on K–Ar and Rb–Sr analyses of minerals and whole-rock samples and conventional multigrain U–Pb zircon analyses, with some Sm–Nd analyses (Liu and others, 1985; Wu and others, 1989; Zhang, Wu, and Ye, 1991; Sun, Armstrong, and Lambert, 1992). Age estimates scatter between 2600 to 1800 Ma, with minor ages older than 2600 Ma or younger than 1800 Ma (Liu and others, 1985). Using conventional isotope dilution techniques on multigrain zircon fractions, Liu and others (1985) obtained a U–Pb date of 2800 +230/-150 Ma (MSWD = 8.6; 95 % conf.) for a paragneiss sample, interpreted as the maximum age of the Fuping Complex. This age, however, was viewed as unreliable because of the unusually large scatter of data points (Sun, Armstrong, and Lambert, 1992). Liu and others (1985) also dated the Lanzhishan granite, which intrudes the Longquanguan augen gneisses of the Fuping Complex. This granite gave an upper intercept age of 2560 ± 6 Ma (MSWD = 2.0; 95 % confidence level), which was interpreted by Liu and others (1985) as a minimum igneous crystallization age for the Fuping Complex. Again, this interpretation was questionable because the Longquanguan gneisses that are intruded by the Lanzhishan granite do not represent the youngest rock unit of the Fuping Complex. Later Rb–Sr, Pb–Pb and Sm–Nd studies indicated the existence of Paleoproterozoic granitic intrusives (for example, the Nanying gneisses in this study) in the Fuping Complex (Sun, Armstrong, and Lambert, 1992; Guan, 2000).

Regional metamorphism of the Fuping Complex was previously considered to have taken place at ~2500 Ma, based on U–Pb dating of euhedral zircons in a feldspathic paragneiss of the Fuping Complex (Liu and others, 1985; Wu and others, 1989). Liu and others (1985) and Wu and others (1989) assigned pink, euhedral, prismatic zircons from the so-called 'feldspathic paragneiss' to metamorphic origins. However, numerous geochronological studies on other metamorphic terrains around the world show that metamorphic zircons are commonly characterized in morphology by either near-spherical and multifaceted single grains or by recrystallization and overgrowth rims on non-metamorphic zircon cores (Kröner and Jaeckel, 1995; Vavra and others, 1996; Vavra, Schmidt, and Gebauer, 1999; Kröner and others, 2000; Pidgeon, Macambira, and Lafon, 2000). In addition, most previously so-called 'feldspathic paragneisses' of the Fuping Complex have been demonstrated to be metamorphosed tonalitic–trondhjemitic–granodioritic plutons (Wang, Li, and Liu, 1991; Liu, 1997). For these reasons, we consider that the euhedral zircon U–Pb upper intercept age of 2470 ± 20 Ma does not represent the true metamorphic age. Therefore, both the igneous crystallization and metamorphic ages of the Fuping Complex have not been well constrained by previous geochronology.

Most recently, the Sensitive High-mass Resolution Ion Micro Probe (SHRIMP) technique has been applied to the dating of the Fuping Complex (Wilde and others, 1997; Guan, 2000). Wilde and others (1997) obtained SHRIMP U–Pb zircon ages of 2543 ± 7 Ma and 2540 ± 18 Ma from the Longquanguan augen gneisses, interpreted as the crystallization ages of the precursor granites. They also obtained a SHRIMP U–Pb zircon age of 1790 ± 8 Ma from a syntectonic pegmatite dike that is interpreted as resulting from the partial melting of the Fuping gneisses (Wilde and others, 1997). This age is considered to approximate the metamorphic age of the Fuping Complex. In addition, Guan (2000) obtained a SHRIMP U–Pb zircon crystallization age of 2708 ± 8 Ma from a hornblende gneiss, which occurs as enclaves in the Fuping gneisses and thus is considered to represent the oldest crust in the Fuping Complex. Whereas these SHRIMP results provide reliable data for some lithologies of the Fuping Complex, significant questions still remain because of a lack of precise and reliable isotopic data for other major lithologies, such as the Nanying gneisses and Wanzi supracrustal rocks. Most importantly, no study has reliably determined the age and duration of regional metamorphism that is crucial for elucidating the tectonic history of the Fuping Complex.

SAMPLE SELECTION AND ANALYTICAL METHODS

Nine samples representing the major lithologies of the Fuping Complex, not dated previously by the SHRIMP, were selected for this geochronological study. Of these, three (FG1, FP217 and FP216) were collected from the Fuping gneisses, two (FP249 and FP260) from the Wanzi supracrustal assemblage, two (FP236 and FP224) from the Longquanguan augen gneisses, and two (FP188-2 and FP204) from the Nanying granitic gneisses. The localities of these samples are shown in figure 3. The petrographic and field descriptions of each sample are given in Appendix A.

The samples were processed by heavy mineral separation involving crushing and initial heavy liquid and subsequent magnetic separation. Samples were divided into size and magnetic fractions using a Frantz isodynamic separator. Zircons from the 105 to 132 and >132 μm non-magnetic fractions were hand-picked and mounted on adhesive tape, enclosed in epoxy resin and then polished to about half their thickness and photographed in reflected and transmitted light, before cathodoluminescence (CL) imaging of zircon grains was carried out using a scanning electron microprobe at Curtin University. The mount was then cleaned and gold-coated. U–Th–Pb analyses were made on the exposed zircon surfaces using the WA consortium SHRIMP II ion microprobe housed at Curtin University, whose instrumental performance has been described by Kennedy and de Laeter (1994). Detailed analytical procedures are described by Compston, Williams, and Meyer (1984) and Nelson (1997). Isotopic ratios are monitored by reference to a $^{206}Pb/^{238}U$ ratios of 0.09432 that is equivalent to an age of 564 Ma for the Sri Lankan gem zircon standard CZ3, fragments of which were mounted with each sample. Pb/U ratios in the unknown samples were corrected using the ln(Pb/U)/ln(UO/U) relationship as measured in standard CZ3. Ages have been calculated from the U and Th decay constants recommended by Steiger and Jäger (1977). All reported ages represent $^{207}Pb/^{206}Pb$ data that have been corrected by the ^{204}Pb technique (Compston, Williams, and Meyer, 1984). Uncertainties in age calculations depend on both counting statistics and the additional effect of the common Pb correction. The common Pb correction was made on the basis of the ^{204}Pb content by assuming a Broken Hill common Pb composition. The analytical data were initially reduced using the computer program KRILL (developed by Peter Kinney at Curtin University) and weighted mean $^{207}Pb/^{206}Pb$ ages for designated groups of analyses were calculated using IsoplotEx 4.96 (Ludwig, 2001). Individual analyses in the data table and concordia plots are present as 1σ error boxes and uncertainties in ages are quoted at the 95 percent confidence level (2σ) unless otherwise indicated.

ZIRCON RESULTS

The interpretation of zircon U–Pb age data depends on distinguishing between detrital, xenocrystic, magmatic and metamorphic zircons, based on their detailed internal structures and U–Th–Pb chemistry (Pupin, 1980; Varva, 1990; Pidgeon, 1992; Vavra and others, 1996; Rowley and others, 1997; Pidgeon and Wilde, 1998; Pidgeon, Nemichin, and Hitchen, 1998; Ashwal, Tucker, and Zinner, 1999; Vavra, Schmidt, and Gebauer, 1999; Bodorkos and others, 2000; Pidgeon, Macambira, and Lafon, 2000). Back-scattered electron (BSE) and cathodoluminescence (CL) imagery have successfully been used to illustrate different growth phases of zircons with a variety of internal structures, especially in recognizing xenocrystic and magmatic cores, and overgrowth and recrystallization rims (Hanchar and Miller, 1993; Hanchar and Rundnick, 1995). CL images tend to show more detailed internal structure than BSE (Hanchar and Rundnick, 1995; Kröner and others, 2000; Pidgeon, Macambira, and Lafon, 2000). In this section, we apply integrated CL images, U–Th chemistry and analysis of SHRIMP zircon geochronology to deduce the complicated magmatic crystallization and metamorphic recrystallization histories of the main lithologies in the Fuping Complex.

Fuping gneisses.—Most zircons in the Fuping gneiss samples FG1, FP216, and FP217 are euhedral and prismatic in morphology as is commonly observed in zircon from magmatic rocks but have been recrystallized or overgrown by thin rims. Based on the CL images, zircons in these samples can be grouped morphologically into three types: (1) grains with concentric, oscillatory zoning (fig. 4A); (2) concentric oscillatory-zoned cores with a narrow (20–50 μm), high luminescent, structureless rim (fig. 4B, C); and (3) high luminescent, nebulously-zoned grains (fig. 4D). Some nebulously-zoned grains have a very narrow (10–20 μm) dark rim (fig. 4D). Based on morphology of these zircons and the assumption that zircon rims generally are younger than the cores that they overgrow, the structureless rims in the type (2) zircons are considered to form by metamorphic recrystallization; the type (1) zircons and oscillatory-zoned cores in type (2) represent magmatic grains; and the type (3) represent either magmatic or metamorphic zircons, but the U–Th chemistry and U–Pb data support the latter interpretation (see below).

SHRIMP zircon U–Th–Pb analytical results from the medium-grained biotite hornblende tonalitic gneiss sample FG1 are included in table 1. Analytical points in this sample were positioned on 11 type (1) zircons, two zoned cores, two structureless rims of type (2) zircons, and three nebulously-zoned grains of type (3). In Th–U chemistry, nebulously-zoned grains and structureless rims are similar; they are all characterized by marked depletion of Th and relatively low abundance of U (<100 ppm) (fig. 5A). On a concordia plot (fig. 6), all analyses on the nebulously-zoned grains and the structureless rims are concordant or only slightly discordant, and define a population with a $^{207}Pb/^{206}Pb$ age of 1802 ± 43 Ma, with a large error. This age is interpreted as approximating the time of metamorphic zircon growth in this sample. The magmatic zircons in types (1) and (2) are higher in Th (up to 344 ppm) and relatively higher in U (up to 1300 ppm), compared to the nebulously-zoned grains and the structureless rims (table 1 and fig. 5A). On the concordia plot, analyses of the magmatic zircons show varying degrees of discordance (fig. 6). Ten of these data points, both concordant and discordant, define a weighted mean $^{207}Pb/^{206}Pb$ age of 2523 ± 14 Ma (fig. 6), interpreted as the crystallization age of the precursor rock of the Fuping tonalitic gneiss. Two data points of the single grains (TA-3 and TA-5) with oscillatory zoning give a weighted mean $^{207}Pb/^{206}Pb$ age of 2351 ± 54 Ma (fig. 6), the geological significance of which remains unknown.

For the trondhjemitic gneiss sample FP217, analytical points were positioned on ten type (1) zircons, four zoned cores and four structureless rims of type (2) zircons, three nebulously-zoned grains and one weakly zoned rim overgrowing a nebulously-

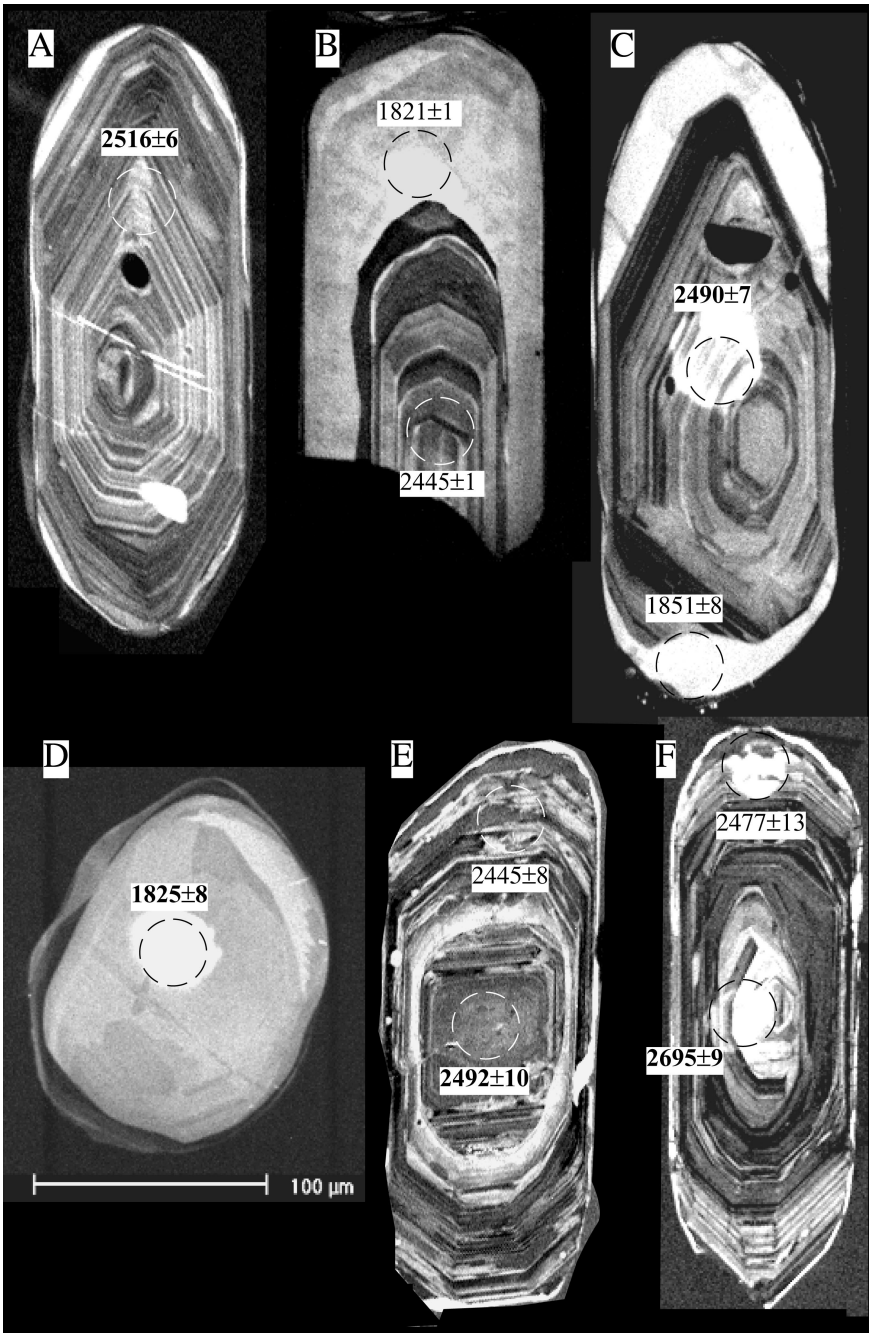

Fig. 4. Representative selection of CL zircon images from the Fuping TTG gneisses and the Longquanguan augen gneisses. Open circles (25-40 μm) show location of SHRIMP analyses, and each spot is labeled with its individual ^{204}Pb-corrected ^{207}Pb/^{206}Pb ages (Ma). A description of zircons is included in the text.

TABLE 1

U–Th–Pb SHRIMP data (with 1σ errors) for tonalitic gneiss sample FG1

Grain Spot	Tex-ture*	U ppm	Th ppm	Th/U	^{204}Pb ppm	% f ^{206}Pb	^{207}Pb** / ^{206}Pb	^{206}Pb** / ^{238}U	^{207}Pb** / ^{235}U	^{207}Pb** / ^{206}Pb Age (Ma)
Ta-1	a	70	0	-	22	2.60	0.110±53	0.302±9	4.58±28	1798±88
Ta-11	a	82	0	-	25	2.87	0.110±52	0.290±9	4.39±26	1795±86
Ta-2	b	100	0	-	33	1.69	0.111±33	0.321±9	4.93±22	1823±54
Ta-17	b	65	0	-	21	0.76	0.108±21	0.333±4	4.96±12	1765±36
Ta-18	b	42	0	-	13	0.53	0.113±24	0.317±4	4.94±13	1848±39
Ta-3	c	82	75	0.91	43	1.20	0.150±31	0.426±13	8.84±35	2351±35
Ta-4	c	294	117	0.4	140	0.54	0.166±13	0.430±12	9.86±29	2521±13
Ta-5	c	91	99	1.08	47	1.64	0.150±39	0.393±12	8.15±34	2350±44
Ta-7	c	281	38	0.14	134	0.50	0.164±11	0.452±12	10.22±30	2497±11
Ta-9	c	561	191	0.34	340	0.15	0.166±6	0.557±15	12.74±35	2516±6
Ta-10	c	95	60	0.63	50	1.97	0.169±32	0.435±13	10.13±37	2547±32
Ta-12	c	417	117	0.28	199	0.09	0.167±5	0.444±3	10.21±7	2524±5
Ta-13	c	634	140	0.22	322	0.04	0.167±3	0.480±3	11.09±7	2533±3
Ta-14	c	1300	344	0.26	663	0.05	0.164±2	0.478±3	10.83±6	2501±2
Ta-15	c	68	58	0.85	41	0.24	0.169±14	0.495±5	11.55±16	2552±14
Ta-16	c	68	33	0.49	37	0.21	0.170±14	0.479±5	11.23±16	2558±14
Ta-6	d	240	26	0.11	86	0.60	0.136±15	0.353±1	6.63±21	2181±19
Ta-8	d	55	8	0.15	33	1.43	0.165±34	0.548±17	12.46±49	2508±35

*a, high-luminescent structureless rims; b, highly luminescent, nebulously-zoned grains; c, single grains with oscillatory zoning; d, oscillatorily zoned cores; e, extremely low luminescent, weakly zoned rims overgrowing structureless single grains.

**corrected for ^{204}Pb. % f^{206}Pb, common ^{206}Pb as a percentage of total ^{206}Pb.

zoned grain (table 2). Like those in sample FG1, nebulously-zoned grains and structureless rims are surprisingly similar in Th–U chemistry; they are lower in Th (<50 ppm) and U (<500 ppm) concentrations and Th/U ratios than other morphological types of zircons (fig. 5B). Differences in Th and U contents between metamorphic and magmatic zircons may result from the selective partitioning of Th and U into the fluid that accompanied the regional amphibolite to granulite facies metamorphism and recrystallization of new zircons. On a concordia plot, all analyses on the nebulously-zoned grains and structureless rims are concordant or slightly discordant, and define a population with a ^{207}Pb/^{206}Pb age of 1875 ± 43 Ma (fig. 7A), which is interpreted as approximating the age of regional metamorphism. In contrast, the types (1) and (2) magmatic zircons contain high Th (up to 675 ppm) and U (up to 1257 ppm) contents and have high Th/U ratios (fig. 5B). On the concordia plot, analyses of magmatic zircon are variably discordant, and ages are not clearly defined, with the main group of nearly concordant data points scattering between 2412 and 2518 Ma (fig. 7A). The spread of data points may reflect later Pb loss. Two analyses on the single grains with oscillatory zoning (Tr-3 and Tr-11) are nearly concordant and yielded a ^{207}Pb/^{206}Pb age of 2499 ± 6 Ma (fig. 7A), which is interpreted as the crystallization age of precursor rocks of the trondhjemitic gneiss. Three data points (Tr-13, 16, and 22) of single grains with oscillatory zoning define a weighted mean ^{207}Pb/^{206}Pb age of 2336 ±

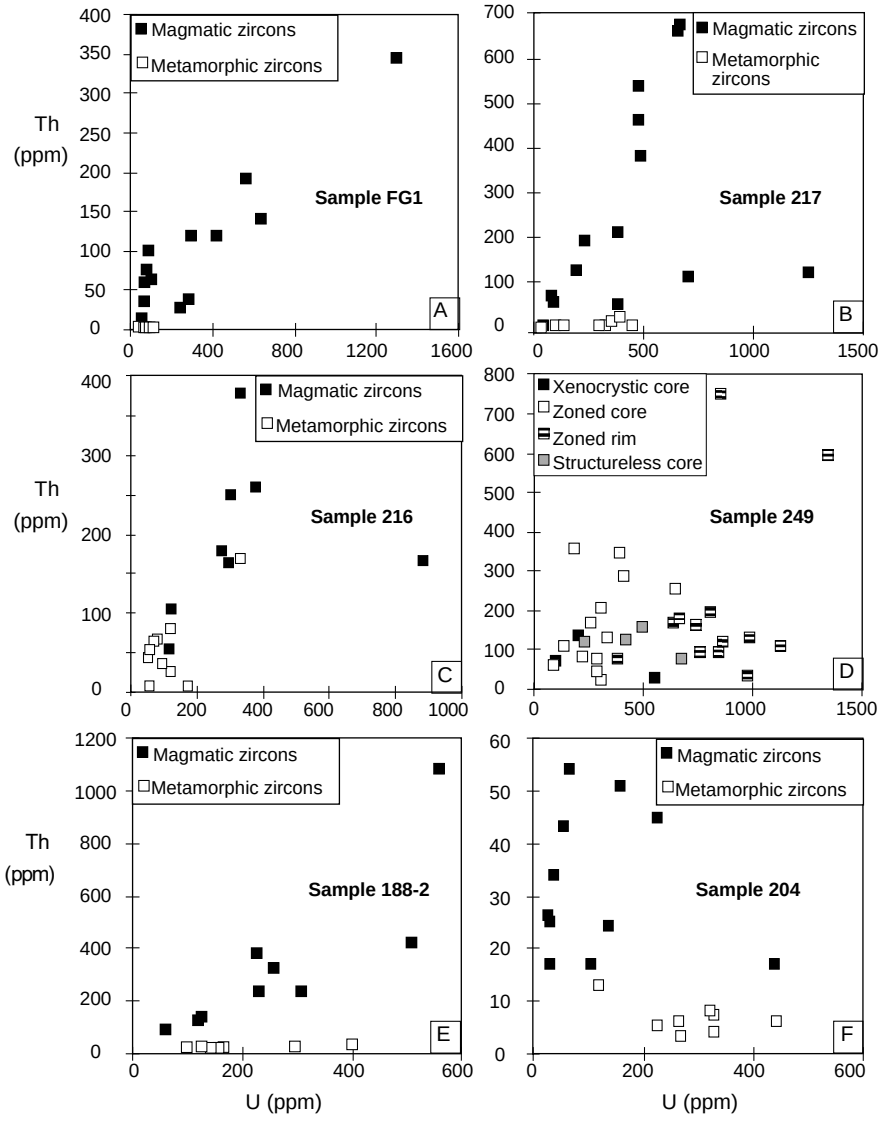

Fig. 5. Plots of U vs Th for the magmatic and metamorphic zircons analyzed in the present study.

9 Ma (fig. 7A), which is much closer to the discordant age of 2351 ± 54 Ma defined by the same type of zircons in sample FG1. A single analysis (Tr-19) on the weakly zoned rim overgrowing a nebulously-zoned grain is strongly discordant and yielded a discordant $^{207}Pb/^{206}Pb$ age of 1633 ± 18 Ma, but whether it records a real event remains unknown.

SHRIMP analyses on the fine-grained biotite granodioritic gneiss sample FP216 were made on five type (1) zircon grains, four oscillatorily-zoned cores and four structureless rims of type (2) zircons, and five type (3) zircon grains (table 3). As shown in figure 4C, most metamorphic zircons (nebulously-zoned grains and structureless rims) are characterized by lower Th (<100 ppm) and U (<200 ppm) concentrations

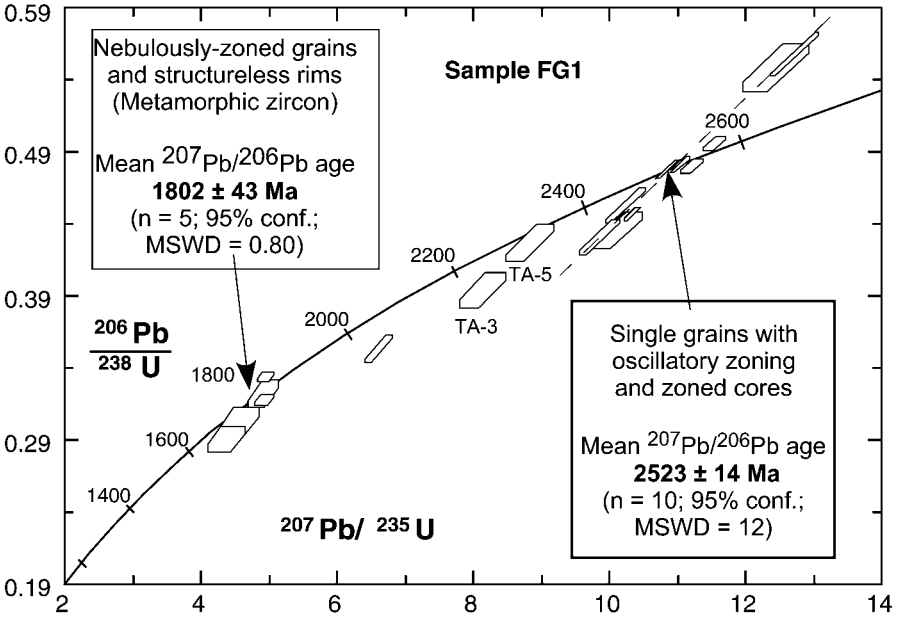

Fig. 6. Concordia plots of SHRIMP U–Pb zircon analytical results for tonalitic gneiss sample FG1.

and Th/U ratios than magmatic zircons. On a concordia plot, seven of the nine analyses on the nebulously-zoned grains and structureless rims form a single, well-defined, concordant population with a $^{207}Pb/^{206}Pb$ age of 1825 ± 12 Ma (fig. 7B), interpreted as the time of metamorphic zircon growth in the Fuping Complex. The other two structureless rims (Gr-9 and Gr-18) are strongly discordant, but fall on a discordia which intersects concordia at an age similar to that defined by the concordant data points (fig. 7B). Compared with the nebulously-zoned grains and structureless rims, the magmatic zircons are obviously higher in Th and U (fig. 5C). On the concordia plot, analyses of the magmatic zircons show $^{207}Pb/^{206}Pb$ ages scattering between 1900 and 2500 Ma (table 3). Four analyses on the single grains with oscillatory zoning form a concordant group with a $^{207}Pb/^{206}Pb$ age of 2486 ± 8 Ma (fig. 7B), interpreted as the crystallization age of the source rock of the granodioritic gneiss. One analysis (Gr-16) on an oscillatory zoned grain also falls lower on concordia and has a $^{207}Pb/^{206}Pb$ age of 2377 ± 11 Ma (1σ), which is comparable to the discordant ages of 2351 ± 54 Ma and 2336 ± 9 Ma defined by the same morphological type of zircons in samples FG1 and FP217, respectively.

Longquanguan augen gneisses.—Zircons from augen gneiss samples FP236 and FP224 form a homogeneous population of euhedral to subhedral prisms with sharp terminations, evidently of igneous origin. The internal structures of the zircons revealed by CL images are characterized by large oscillatorily-zoned cores and extremely narrow (<10 mm) structureless rims with high luminescence (fig. 4E and F). The structureless rims are interpreted to result from metamorphic recrystallization or overgrowth, whereas the zoned cores formed during magmatic crystallization, as described for samples FG1, FP216, and FP217. A few zircon grains in sample FP236 contain small unzoned or weakly zoned, relatively high luminescent cores that may represent xenocrystic zircons (fig. 4F).

Ion microprobe data from the biotite augen gneiss sample FP236 are summarized in table 4. As the structureless rims in this sample are too narrow to be analyzed,

TABLE 2

U–Th–Pb SHRIMP data (with 1σ errors) for trondhjemitic gneiss sample FP217

Grain Spot	Tex-ture*	U ppm	Th ppm	Th/U	^{204}Pb ppm	% f ^{206}Pb	$^{207}Pb/^{206}Pb$ **	$^{206}Pb/^{238}U$ **	$^{207}Pb/^{235}U$ **	$^{207}Pb/^{206}Pb$ ** Age (Ma)
Tr-7	a	329	1	0.00	144	8.27	0.117±25	0.332±61	5.34±16	1906±39
Tr-8	a	104	2	0.02	32	0.31	0.111±15	0.316±62	4.83±12	1816±25
Tr-9	a	141	1	0.00	48	0.34	0.114±11	0.350±67	5.51±12	1867±17
Tr-10	a	358	14	0.04	113	0.06	0.113±5	0.325±59	5.07±10	1851±8
Tr-4	b	454	1	0.00	192	5.84	0.115±19	0.352±64	5.59±14	1883±29
Tr-17	b	299	5	0.02	97	0.12	0.115±6	0.333±61	5.26±10	1875±9
Tr-21	b	32	0	0.01	11	0.51	0.122±31	0.344±82	5.80±21	1991±45
Tr-1	c	194	126	0.65	85	0.75	0.160±14	0.370±70	8.18±18	2460±14
Tr-3	c	387	212	0.55	202	0.00	0.164±5	0.461±84	10.42±20	2498±5
Tr-5	c	1257	121	0.10	437	10.16	0.126±18	0.239±43	4.14±10	2040±26
Tr-6	c	382	49	0.13	182	0.62	0.159±7	0.448±81	9.83±19	2448±8
Tr-11	c	41	2	0.05	19	0.14	0.166±20	0.461±102	10.55±28	2518±21
Tr-13	c	668	675	1.01	276	2.93	0.149±13	0.308±55	6.34±13	2336±15
Tr-14	c	710	112	0.16	342	0.10	0.161±4	0.460±83	10.24±19	2469±4
Tr-15	c	87	53	0.60	45	0.21	0.156±14	0.453±91	9.74±22	2414±15
Tr-16	c	480	461	0.96	206	0.77	0.148±7	0.367±66	7.51±14	2326±9
Tr-20	c	488	382	0.78	268	0.19	0.162±5	0.459±83	10.26±19	2475±5
Tr-2	d	232	191	0.82	125	0.02	0.163±7	0.448±82	10.09±20	2490±7
Tr-12	d	662	660	1.00	307	1.11	0.159±7	0.384±69	8.39±16	2442±8
Tr-18	d	82	68	0.83	32	1.06	0.135±23	0.339±68	6.33±18	2168±30
Tr-22	d	483	538	1.11	205	0.17	0.150±5	0.336±61	6.93±13	2341±6
Tr-19	e	391	23	0.06	70	0.39	0.100±10	0.153±28	2.12±5	1633±18

*a, high-luminescent structureless rims; b, highly luminescent, nebulously-zoned grains; c, single grains with oscillatory zoning; d, oscillatorily zoned cores; e, extremely low luminescent, weakly zoned rims overgrowing structureless single grains.

**corrected for ^{204}Pb. % $f^{206}Pb$, common ^{206}Pb as a percentage of total ^{206}Pb.

analyses were concentrated on the zoned cores, except one analysis (Mg-12) of a xenocrystic core. On a concordia plot (fig. 8A), analyses on the zoned cores are variably discordant, with uranium contents of 137 to 1228 ppm, Th contents of 78 to 1237 ppm, and $^{207}Pb/^{206}Pb$ ages within the range 1850 to 2590 Ma (table 4). Using IsoplotEx, a York (1969) regression through 15 data-points of the zoned cores defines an upper intercept age of 2510 ± 22 Ma (fig. 8A, inset). This age is interpreted as the crystallization age of the magmatic protoliths of the biotite augen gneiss. The xenocrystic core (Mg-12) is nearly concordant, with comparatively low U (324 ppm) and Th (195 ppm) contents and a $^{207}Pb/^{206}Pb$ age of 2695 ± 9 Ma (fig. 8A), markedly older than the ages of the zoned cores.

Sample 224 is a mylonitized granitic pegmatite dike which intrudes the biotite augen gneiss (sample FP236). Data obtained from this sample are presented in table 5, and a concordia plot for all 20 analyses is shown in figure 8B. As the recrystallization rims are too narrow to be analyzed and no xenocrystic cores are suitable for analysis, all

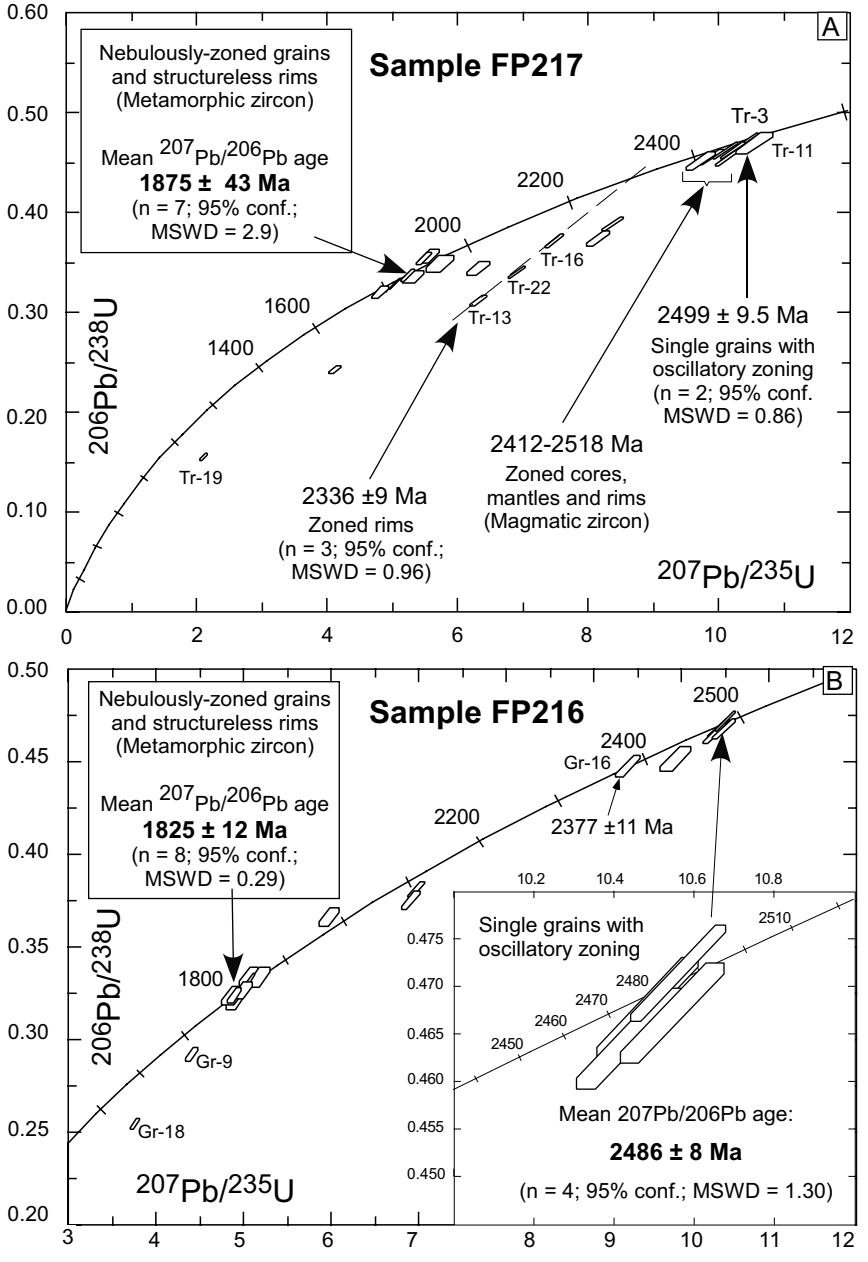

Fig. 7. Concordia plots of SHRIMP U–Pb zircon analytical results for trondhjemitic gneiss sample FP217 (A) and granodioritic gneiss sample FP216 (B).

analyses were positioned on the zoned cores. Data-points are relatively strongly correlated and a York regression through all 20 data-points, using the program IsoplotEx, defines an upper intercept age of 2507 ± 11 Ma (fig. 8B), which approximates the age of crystallization of the deformed granitic pegmatite dike. The age is not significantly different from the approximate crystallization age determined for the

TABLE 3

U–Th–Pb SHRIMP data (with 1σ errors) for granodioritic gneiss sample FP216

Grain Spot	Tex-ture*	U ppm	Th ppm	$\frac{Th}{U}$	^{204}Pb ppm	% f ^{206}Pb	$\frac{^{207}Pb}{^{206}Pb}$ **	$\frac{^{206}Pb}{^{238}U}$ **	$\frac{^{207}Pb}{^{235}U}$ **	$\frac{^{207}Pb}{^{206}Pb}$ ** Age (Ma)
Gr-7	a	51	44	0.85	20	0.54	0.111±21	0.323±51	4.95±13	1818±35
Gr-9	a	120	25	0.21	35	0.16	0.110±11	0.291±38	4.43±8	1805±18
Gr-12	a	124	82	0.67	45	0.00	0.111±10	0.322±42	4.94±8	1821±16
Gr-13	a	55	3	0.05	18	0.21	0.113±18	0.333±53	5.21±12	1856±28
Gr-2	b	63	56	0.89	24	0.30	0.112±17	0.320±48	4.92±11	1826±28
Gr-5	b	74	65	0.88	29	0.24	0.111±15	0.333±49	5.09±11	1810±24
Gr-6	b	77	69	0.89	30	0.33	0.112±16	0.325±47	5.01±11	1826±26
Gr-17	b	332	168	0.51	119	0.00	0.112±5	0.331±38	5.10±6	1825±8
Gr-18	b	302	250	0.83	89	0.12	0.108±7	0.254±29	3.78±5	1767±11
Gr-3	c	381	258	0.68	208	0.02	0.163±5	0.468±53	10.49±13	2484±5
Gr-8	c	177	6	0.04	66	0.03	0.133±8	0.379±46	6.97±10	2141±11
Gr-10	c	277	178	0.64	149	0.04	0.163±6	0.464±54	10.44±13	2488±6
Gr-11	c	328	378	1.15	196	0.02	0.164±6	0.467±53	10.55±13	2496±6
Gr-14	c	884	167	0.19	436	0.03	0.163±3	0.471±51	10.56±12	2483±3
Gr-1	d	300	167	0.56	129	0.02	0.132±6	0.385±44	7.03±9	2130±8
Gr-4	d	122	56	0.46	62	0.39	0.159±15	0.456±65	9.99±18	2445±16
Gr-15	d	94	36	0.38	37	0.43	0.120±15	0.363±50	6.00±12	1955±22
Gr-16	d	123	105	0.86	66	0.03	0.153±10	0.449±58	9.45±14	2377±11

*a, high-luminescent structureless rims; b, highly luminescent, nebulously-zoned grains; c, single grains with oscillatory zoning; d, oscillatorily zoned cores; e, extremely low luminescent, weakly zoned rims overgrowing structureless single grains.

**corrected for ^{204}Pb. % $f^{206}Pb$, common ^{206}Pb as a percentage of total ^{206}Pb.

biotite augen gneiss (sample FP236), which implies that the protoliths of the biotite augen gneiss and granitic pegmatite dike probably formed during the same magmatic event.

Wanzi supracrustal assemblage.—Zircons in the supracrustal rock samples FP249 and FP260 are subhedral, and interpreted to be igneous origin, although most have been rounded and pitted, probably by subsequent sedimentary transport. Unlike those in samples FG1, FP216, FP217, FP236, and FP224, most zircons in samples FP249 and FP260 have minor to no recrystallization or overgrowth rims. The CL images reveal three morphologies of zircons from these samples: (1) a small xenocrystic core truncated by a large zoned rim (fig. 9A); (2) a small zoned core divided from a large zoned rim by a non-luminescent seam (fig. 9B); and (3) a large, low luminescent, structureless core with a narrow (<20 μm), highly luminescent, structureless rim (fig. 9C). Most zircons occur as morphological type (2), whereas types (1) and (3) are rare. Like those in samples FP216 and FP217, the narrow structureless rims with high luminescence are interpreted to be the result of metamorphic recrystallization or overgrowth, whereas the other morphological types represent the detrital zircons of the original sediments, most of which were derived from igneous source rocks, as implied by their prismatic shape. Minor components came from non-igneous sources, as implied by low luminescent, structureless cores in the type (2) zircons.

TABLE 4

U–Th–Pb SHRIMP data (with 1σ errors) for mylonitized granitic pegmatite sample FP224

Grain Spot	Texture*	U ppm	Th ppm	$\frac{Th}{U}$	^{204}Pb ppm	% f ^{206}Pb	$\frac{^{207}Pb}{^{206}Pb}$ **	$\frac{^{206}Pb}{^{238}U}$ **	$\frac{^{207}Pb}{^{235}U}$ **	$\frac{^{207}Pb}{^{206}Pb}$ ** Age (Ma)
Mg-1	a	289	97	0.33	127	0.39	0.163±13	0.404±42	9.09±13	2490±13
Mg-2	a	877	289	0.33	328	0.41	0.159±8	0.342±33	7.51±8	2445±8
Mg-3	a	462	132	0.28	231	0.33	0.163±9	0.462±46	10.42±13	2492±10
Mg-4	a	184	143	0.78	95	0.26	0.163±15	0.428±48	9.61±15	2484±16
Mg-5	a	430	138	0.32	185	0.28	0.158±9	0.398±40	8.67±11	2433±10
Mg-6	a	1228	1237	1.01	303	0.72	0.113±8	0.204±19	3.18±4	1850±13
Mg-7	a	796	243	0.31	286	0.32	0.150±8	0.335±32	6.93±8	2346±9
Mg-8	a	685	170	0.25	375	0.22	0.165±7	0.513±49	11.71±13	2512±7
Mg-9	a	305	223	0.73	168	0.36	0.174±11	0.461±48	11.06±14	2597±11
Mg-10	a	1053	527	0.50	338	0.34	0.139±7	0.288±27	5.52±6	2213±9
Mg-11	a	224	62	0.28	114	0.20	0.162±13	0.473±51	10.57±15	2477±13
Mg-12	b	324	149	0.46	195	0.10	0.185±10	0.533±55	13.56±16	2695±9
Mg-13	a	282	111	0.39	145	0.09	0.167±10	0.468±48	10.77±14	2525±10
Mg-14	a	137	106	0.77	78	0.26	0.164±16	0.477±56	10.81±18	2501±16
Mg-15	a	391	150	0.38	139	0.58	0.151±13	0.321±33	6.69±9	2357±14
Mg-16	a	494	47	0.09	228	0.14	0.162±8	0.450±44	10.07±12	2480±8
Mg-17	a	187	111	0.59	109	1.61	0.164±20	0.485±54	10.99±19	2501±20

*a, oscillatorily zoned zircons; b, xenocrystic core.
**corrected for ^{204}Pb. % $f^{206}Pb$, common ^{206}Pb as a percentage of total ^{206}Pb.

Analytical data for sample FP249 are presented in table 6, and a concordia plot is shown in figure 10A. Of 33 analyses, three were made on small xenocrystic cores truncated by large zoned rims, 13 on the zoned cores, 13 on the zoned rims, and four on the low-luminescent structureless cores. The high-luminescent structureless rims in this sample are too narrow (<20 μm) to be analyzed. As shown in figure 5D, most zoned rims have higher U concentrations than the zoned cores, but their Th variation is not as pronounced. On a concordia plot, although most analyses of the zoned cores and all analyses of the zoned rims are strongly discordant, five analyses on the zoned cores form a concordant group with a $^{207}Pb/^{206}Pb$ age of 2502 ± 5 Ma (fig. 10A, inset), interpreted as the crystallization age of igneous source rocks contributing to the supracrustal rock. This conclusion is supported by the strong correlation of ten analyses on the zoned cores, which define a York fit upper intersection age of 2502 ± 7 Ma (MSWD = 1.09). Xenocrystic cores have U and Th concentrations similar to those of the zoned cores (fig. 5D). Three analyses on the xenocrystic cores give a weighted mean $^{207}Pb/^{206}Pb$ age of 2554 ± 8 Ma (MSWD = 0.48), markedly older than that of the zoned cores. Two of four analyses on the low-luminescent structureless cores form a nearly concordant group with a weighted mean $^{207}Pb/^{206}Pb$ age of 2460 ± 60 Ma (MSWD = 1.4), significantly younger than the concordant age defined by the zoned cores. A zoned zircon grain (Sg-19) has a near concordant age of 2109 ± 5 Ma (1σ), which may provide a maximum depositional age for the Wanzi supracrustals. This conclusion is supported by Guan (2000) who obtained a SHRIMP U–Pb zircon age of 2097 ± 46 Ma from the fine-grained paragneiss of the Wanzi supracrustals.

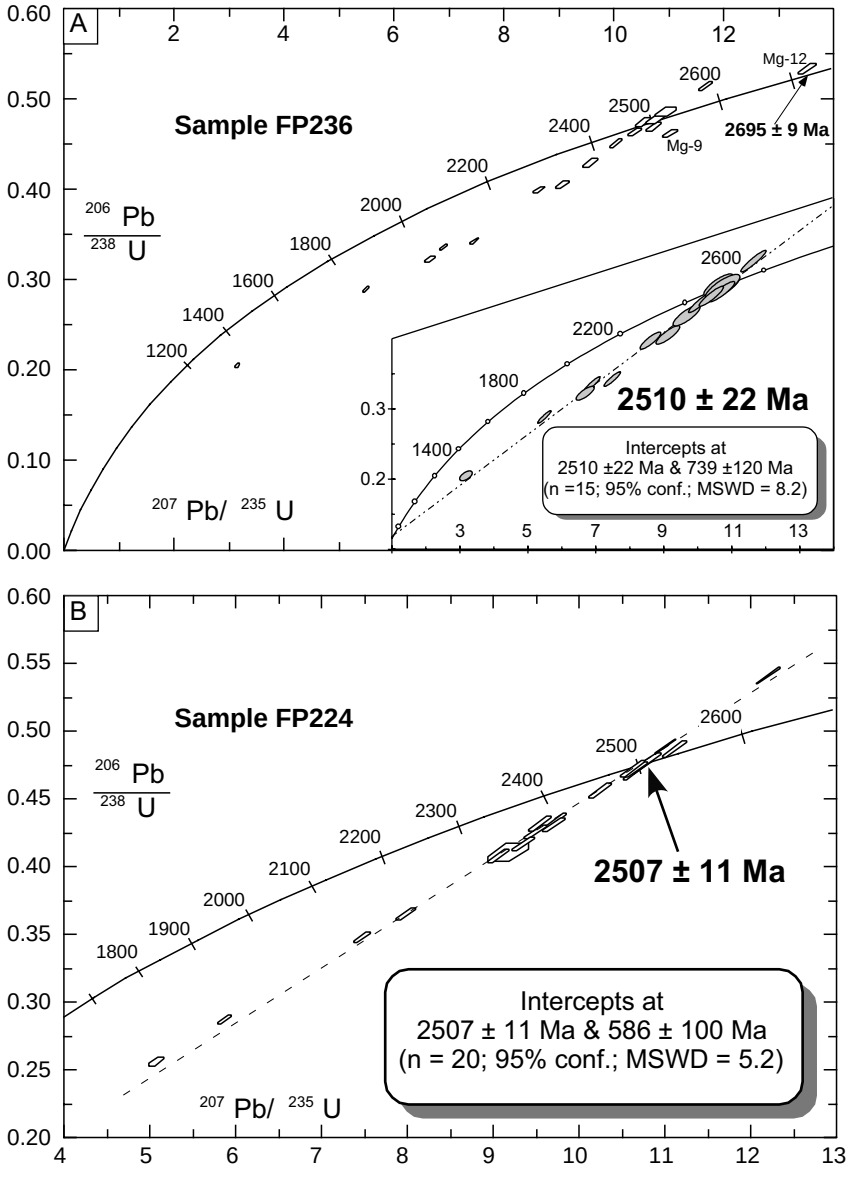

Fig. 8. Concordia plots of SHRIMP U–Pb zircon analytical results for the Longquanguan augen gneisses of the Fuping Complex. (A) Monzogranitic gneiss (sample FP236); (B) Mylonitized granitic pegmatite dike (sample FP224).

Table 7 lists SHRIMP analytical results of zircons in sample FP260 in which analytical areas were positioned on two xenocrystic cores, eight zoned cores, eight zoned rims, and two low-luminescent structureless cores. The Th–U contents of various morphological types of zircons are similar to those in sample FP249. On a concordia plot, nearly all analyses of the zoned cores and rims are strongly discordant, with the zoned rims being more discordant and having lower apparent $^{207}Pb/^{206}Pb$ ages than the zoned cores (fig. 10B). Of eight analyses of the zoned cores, data points Sl-2 and

TABLE 5

U–Th–Pb SHRIMP data (with 1σ errors) for mylonitized granitic pegmatite sample FP224

Grain Spot	Texture*	U ppm	Th ppm	Th/U	^{204}Pb ppm	% f ^{206}Pb	^{207}Pb** / ^{206}Pb	^{206}Pb** / ^{238}U	^{207}Pb** / ^{235}U	^{207}Pb** / ^{206}Pb Age (Ma)
Pg-1	a	564	392	0.70	311	0.06	0.165±5	0.469±56	10.70±14	2510±5
Pg-2	a	484	253	0.52	238	0.22	0.163±6	0.432±52	9.73±13	2490±6
Pg-3	a	475	402	0.85	270	0.09	0.165±5	0.474±57	10.79±14	2509±6
Pg-4	a	2480	487	0.20	1408	0.07	0.164±2	0.540±62	12.25±14	2502±2
Pg-5	a	731	743	1.02	238	0.90	0.142±13	0.259±32	5.06±8	2246±15
Pg-6	a	492	403	0.82	251	0.18	0.163±6	0.425±52	9.53±13	2484±6
Pg-7	a	497	303	0.61	239	0.17	0.164±7	0.416±51	9.39±13	2493±7
Pg-8	a	269	158	0.59	147	0.00	0.165±7	0.478±61	10.86±15	2506±7
Pg-9	a	583	507	0.87	307	0.10	0.164±5	0.433±52	9.77±13	2493±5
Pg-10	a	361	197	0.54	193	0.05	0.165±6	0.471±58	10.70±14	2505±6
Pg-11	a	604	479	0.79	313	0.42	0.161±6	0.431±52	9.59±13	2469±7
Pg-12	a	584	501	0.86	249	0.64	0.157±8	0.347±42	7.50±10	2420±9
Pg-13	a	406	259	0.64	215	0.16	0.164±6	0.456±56	10.29±14	2496±6
Pg-14	a	507	402	0.79	249	0.28	0.162±7	0.408±49	9.10±12	2477±7
Pg-15	a	700	661	0.94	248	0.53	0.147±7	0.290±35	5.88±8	2311±8
Pg-16	a	422	287	0.68	232	0.04	0.164±5	0.472±57	10.67±14	2499±6
Pg-17	a	550	474	0.86	248	0.78	0.159±8	0.365±44	8.02±11	2450±9
Pg-18	a	418	254	0.61	194	0.00	0.163±29	0.410±67	9.21±23	2488±30
Pg-19	a	556	433	0.78	322	0.13	0.166±5	0.486±58	11.16±14	2522±5
Pg-20	a	2302	586	0.25	1193	0.01	0.164±2	0.488±56	11.06±13	2500±2

*a, oscillatorily zoned zircons; b, xenocrystic core.
**corrected for ^{204}Pb. % f^{206}Pb, common ^{206}Pb as a percentage of total ^{206}Pb.

Sl-16 contain too much higher and lower Th/U ratios, respectively, compared with other data-points (table 7). The other 6 data points of the zoned cores show a strong correlation and fall on a common chord that intersects Concordia at 2507 ± 14 Ma and 227 ± 240 Ma (2σ and MSWD = 0.81). The upper intersection age of 2507 ± 14 Ma is comparable to the age of 2502 ± 3 defined by the zoned cores in sample FP249 and is considered to approximate the crystallization age of the igneous source rocks. All analyses on the zoned rims are strongly discordant, and ages are not clearly defined (fig. 10B). Of the two xenocrystic cores analyzed, one (Sl-17) yielded a concordant ^{207}Pb/^{206}Pb age of 2827 ± 8 Ma (fig. 10B), which, as far as we are aware, is the oldest single-grain zircon age reported from the Fuping Complex. The other one (Sl-19) yielded a concordant ^{207}Pb/^{206}Pb age of 2686 ± 6 Ma (fig. 9A and fig. 10B), also markedly older than the age of the zoned cores. Two analyses on the low-luminescent structureless cores are strongly discordant and ages are not clearly defined.

Nanying granitic gneisses.—Zircons in the Nanying granitic gneiss samples FP188-2 and FP204 can be classified into three morphological types. Type (1) consists of anhedral zircons with weakly zoned or unzoned cores and structureless rims (fig. 9D, E). The rims are highly luminescent and truncate the internal growth bands of the weakly zoned cores (fig. 9D). Type (2) consists of euhedral, prismatic zircons with

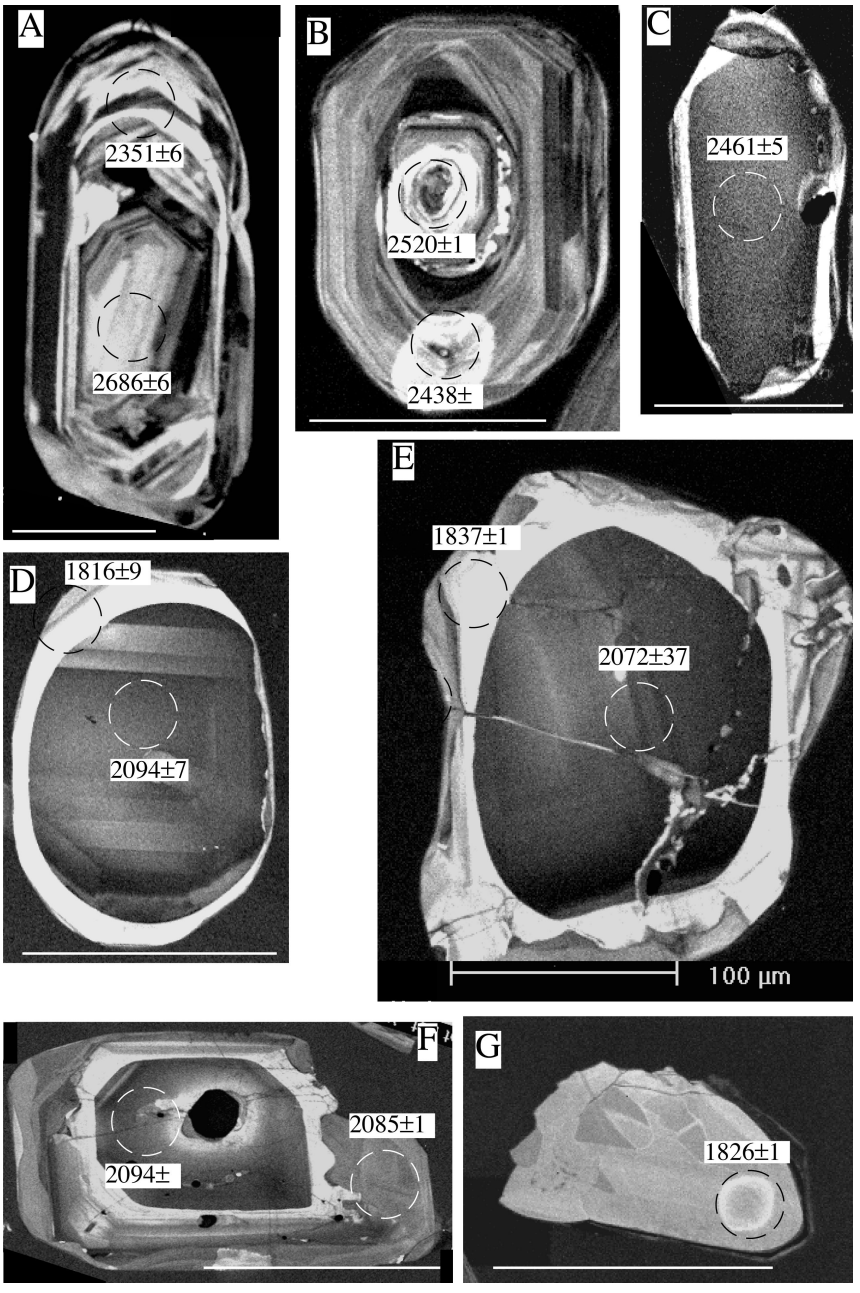

Fig. 9. Representative selection of CL zircon images from the Wanzi supracrustal series and the Nanying gneisses. Open circles (25-40μm) show location of SHIRMP analyses, and each spot is labeled with its individual ^{204}Pb-corrected ^{207}Pb/^{206}Pb ages (Ma). A description of zircons is included in the text. All scale bars = 100 μm.

unzoned or weakly zoned cores divided from faintly zoned rims by a narrow (<20 μm) high-luminescent seams (fig. 9F). The unzoned or weakly zoned cores have zoning bands and CL intensity similar to those cores of type (1) zircons. The high-luminescent

TABLE 6

U–Th–Pb SHRIMP data (with 1σ errors) for sillimanite gneiss sample FP249

Grain Spot	Texture*	U ppm	Th (ppm)	U/Th	^{204}Pb (ppm)	% f ^{206}Pb	^{207}Pb** / ^{206}Pb	^{206}Pb** / ^{238}U	^{207}Pb** / ^{235}U	^{207}Pb** / ^{206}Pb Age (Ma)
Sg-1	a	182	355	1.95	111	0.32	0.166±15	0.415±83	9.48±22	2517±15
Sg-2	a	308	22	0.07	129	0.41	0.163±12	0.407±8	9.13±19	2485±13
Sg-3	a	287	40	0.14	123	0.13	0.165±10	0.413±78	9.38±19	2506±10
Sg-5	a	293	74	0.25	114	1.07	0.150±18	0.352±7	7.30±17	2351±20
Sg-6	a	395	343	0.87	173	2.20	0.160±22	0.339±63	7.47±18	2453±23
Sg-9	a	265	165	0.62	123	0.25	0.166±13	0.399±76	9.10±19	2514±13
Sg-13	a	409	285	0.70	166	0.32	0.166±10	0.345±63	7.91±16	2520±10
Sg-18	a	652	253	0.39	336	0.03	0.164±4	0.469±81	10.63±19	2502±4
Sg-20	a	226	80	0.36	109	0.14	0.152±6	0.442±78	9.26±17	2368±7
Sg-21	a	313	202	0.65	179	0.14	0.164±5	0.492±86	11.14±20	2502±5
Sg-22	a	136	108	0.80	79	0.20	0.164±9	0.479±87	10.86±21	2502±9
Sg-30	a	341	129	0.38	186	0.14	0.164±5	0.496±87	11.23±20	2499±5
Sg-31	a	95	56	0.59	52	0.14	0.165±12	0.471±89	10.73±23	2510±12
Sg-7	b	746	160	0.21	258	2.31	0.154±16	0.299±53	6.37±14	2396±18
Sg-8	b	1348	591	0.44	390	4.18	0.126±16	0.231±40	3.99±9	2037±22
Sg-4	b	1134	106	0.09	383	3.69	0.145±16	0.288±50	5.75±13	2287±19
Sg-10	b	645	167	0.26	220	1.72	0.148±14	0.307±55	6.25±13	2322±16
Sg-11	b	665	177	0.27	276	0.49	0.161±8	0.383±69	8.52±16	2470±9
Sg-12	b	848	90	0.11	340	0.34	0.158±7	0.385±68	8.41±16	2438±7
Sg-14	b	873	118	0.13	362	0.59	0.157±8	0.395±70	8.55±16	2425±8
Sg-15	b	858	747	0.87	319	7.65	0.111±26	0.255±46	3.91±12	1821±42
Sg-17	b	388	75	0.19	146	0.47	0.138±6	0.354±62	6.76±13	2208±8
Sg-19	b	983	30	0.03	377	0.46	0.131±4	0.383±66	6.91±12	2109±5
Sg-27	b	765	89	0.12	355	0.99	0.155±5	0.435±75	9.28±17	2398±6
Sg-28	b	991	127	0.13	310	7.85	0.119±15	0.234±41	3.86±9	1949±23
Sg-32	b	811	192	0.24	381	1.25	0.159±6	0.425±73	9.29±17	2442±7
Sg-16	c	556	25	0.05	251	0.80	0.170±6	0.429±74	10.05±18	2558±6
Sg-23	c	206	135	0.65	117	0.09	0.169±7	0.485±86	11.30±21	2549±7
Sg-24	c	96	67	0.70	55	0.07	0.170±10	0.484±89	11.31±23	2554±10
Sg-25	d	425	122	0.29	186	0.68	0.151±7	0.394±69	8.21±15	2360±8
Sg-26	d	232	115	0.49	126	0.18	0.161±6	0.483±86	10.76±20	2471±7
Sg-29	d	502	156	0.31	212	1.27	0.155±9	0.370±65	7.92±15	2405±10
Sg-33	d	676	75	0.11	344	0.45	0.161±5	0.486±85	10.75±19	2461±5

*a, zoned cores; b, zoned rims; c, xenocrystic cores; d, low-luminescent structureless cores.
**corrected for ^{204}Pb. % f^{206}Pb, common ^{206}Pb as a percentage of total ^{206}Pb.

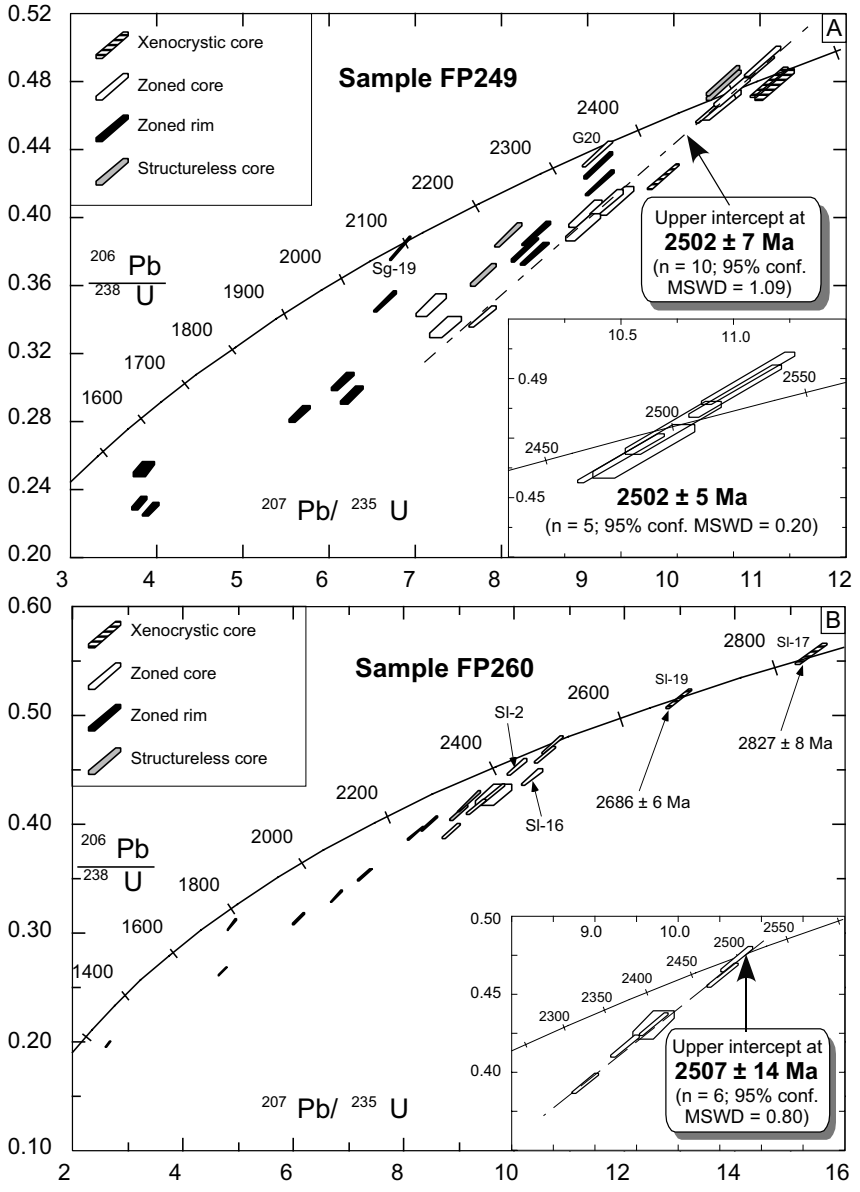

Fig. 10. Concordia plots of SHRIMP zircon U-Pb analytical results for rocks from the Wanzi supracrustal series. (A) Sillimanite gneiss sample FP249; (B) Sillimanite gneiss sample FP260.

seams show weakly zoned bands (fig. 9F) and are similar in CL intensity to the structureless rims of the type (1) zircons (fig. 9D, E). Type (3) consists of high-luminescent, nebulously-zoned grains (fig. 9G). Like our interpretation for the other samples from the Fuping Complex, the unzoned or weakly zoned cores in types (1) and (2) represent either magmatic grains or xenocrysts, whereas the highly luminescent, structureless rims of type (1) and nebulously-zoned grains of type (3) resulted from metamorphic recrystallization or overgrowth. In type (2), the faintly zoned rims

TABLE 7

U–Th–Pb SHRIMP data (with 1σ errors) for sillimanite leptynite samples FP260

Grain Spot	Texture*	U ppm	Th (ppm)	U/Th	^{204}Pb (ppm)	% f ^{206}Pb	^{207}Pb** / ^{206}Pb	^{206}Pb** / ^{238}U	^{207}Pb** / ^{235}U	^{207}Pb** / ^{206}Pb Age (Ma)
Sl-2	a	272	679	2.50	197	0.58	0.162±81	0.452±77	10.09±19	2477±8
Sl-5	a	304	47	0.15	150	0.14	0.165±63	0.472±80	10.72±19	2503±6
Sl-7	a	293	89	0.30	135	0.25	0.164±59	0.431±73	9.71±17	2494±6
Sl-11	a	309	238	0.77	152	0.54	0.163±78	0.416±71	9.34±17	2487±8
Sl-12	a	42	40	0.94	23	1.38	0.164±374	0.426±95	9.67±33	2502±38
Sl-14	a	291	101	0.35	147	0.13	0.166±61	0.464±79	10.60±19	2516±6
Sl-16	a	202	54	0.27	93	0.35	0.172±94	0.441±76	10.42±20	2572±9
Sl-18	a	450	315	0.70	205	0.36	0.164±67	0.393±66	8.89±16	2499±7
Sl-3	b	611	175	0.29	219	0.25	0.148±53	0.333±56	6.80±12	2324±6
Sl-1	b	2056	14	0.01	410	1.75	0.098±58	0.197±33	2.66±5	1580±11
Sl-8	b	1543	424	0.27	431	0.73	0.130±45	0.264±44	4.73±8	2097±6
Sl-9	b	944	152	0.16	388	0.42	0.153±43	0.391±65	8.25±14	2378±5
Sl-10	b	810	99	0.12	258	0.09	0.142±38	0.312±52	6.12±11	2251±5
Sl-13	b	1217	35	0.03	369	0.46	0.116±38	0.307±51	4.90±8	1891±6
Sl-15	b	647	42	0.06	262	0.17	0.154±43	0.400±67	8.49±15	2391±5
Sl-20	b	871	61	0.07	314	0.33	0.150±50	0.353±59	7.32±13	2351±6
Sl-17	c	144	78	0.54	94	0.20	0.200±93	0.561±99	15.49±29	2827±8
Sl-19	c	212	156	0.73	131	0.06	0.184±65	0.515±89	13.03±23	2686±6
Sl-4	d	457	218	0.48	212	0.53	0.160±73	0.410±69	9.04±16	2455±8
Sl-6	d	697	71	0.10	303	0.14	0.159±39	0.423±70	9.29±16	2450±4

*a, zoned cores; b, zoned rims; c, xenocrystic cores; d, low-luminescent structureless cores.
**corrected for ^{204}Pb. % f^{206}Pb, common ^{206}Pb as a percentage of total ^{206}Pb.

represent magmatic zonation, and the high-luminescent seams represent recrystallized zircons.

Table 8 summarizes the SHRIMP U–Th–Pb data for monzogranitic gneiss sample FP188-2. Analyses were made on five unzoned or weakly zoned cores of types (1) and (2) zircons, four zoned rims of type (2) zircons, five structureless rims of type (1) zircons and two nebulously-zoned grains of type (3) zircons. The high-luminescent seams in type (2) zircons are too narrow to be analyzed. The SHRIMP analyses show that the structureless rims of type (1) zircons have U and Th concentrations and Th/U ratios similar to those of the nebulously-zoned grains of type (3); whereas unzoned or weakly zoned cores of types (1) and (2) zircons have U and Th contents and Th/U ratios similar to those of zoned rims of type (2) zircons. On a U versus Th plot, the distinction between the metamorphic zircons (nebulously-zoned grains and structureless rims) and magmatic zircons (unzoned or weakly zoned cores and zoned rims) is obvious (fig. 5E). Although the U concentrations of all types of zircons range from 62 to 562 ppm, the Th contents of the metamorphic zircons (2 to 26 ppm) are markedly lower than those of magmatic zircons (83 to 1083 ppm). On a concordia plot, nine analyses on the unzoned or weakly zoned cores of types (1) and (2) zircons and the zoned rims of type (2) zircons define a statistically simple concordant population with

TABLE 8

U–Th–Pb SHRIMP data (with 1σ errors) for monzogranitic gneiss sample FP188-2

Grain Spot	Tex-ture*	U ppm	Th ppm	U/Th	204Pb ppm	% f 206Pb	207Pb/206Pb **	206Pb/238U **	207Pb/235U **	207Pb/206Pb ** Age (Ma)
Mz-1	a	509	421	0.83	233	0.02	0.130±5	0.391±47	6.99±9	2094±7
Mz-2	a	125	138	1.11	59	0.35	0.126±13	0.375±53	6.51±12	2039±18
Mz-3	a	62	83	1.34	30	0.64	0.127±21	0.373±61	6.53±16	2056±30
Mz-4	a	259	318	1.23	124	0.23	0.129±9	0.373±48	6.61±10	2079±12
Mz-7	a	562	1083	1.93	310	0.04	0.130±5	0.380±46	6.80±9	2094±7
Mz-10	b	228	376	1.64	119	0.25	0.127±9	0.375±48	6.59±10	2064±12
Mz-11	b	308	233	0.76	134	0.29	0.129±8	0.374±47	6.64±10	2081±11
Mz-13	b	125	145	1.16	60	0.22	0.126±13	0.374±53	6.52±12	2050±19
Mz-15	b	233	231	0.99	109	0.07	0.129±8	0.383±49	6.82±10	2085±11
Mz-5	c	165	5	0.03	53	0.29	0.113±11	0.329±44	5.12±9	1845±18
Mz-6	c	402	26	0.06	129	0.05	0.111±6	0.328±40	5.02±7	1816±9
Mz-12	c	127	15	0.12	44	0.47	0.115±14	0.346±49	5.49±11	1882±22
Mz-14	c	158	3	0.02	49	0.25	0.113±13	0.321±44	5.01±9	1853±20
Mz-16	c	141	7	0.05	48	0.27	0.116±13	0.349±48	5.58±11	1892±21
Mz-8	d	296	24	0.08	96	0.16	0.112±7	0.332±42	5.11±8	1826±11
Mz-9	d	101	2	0.02	34	0.70	0.111±19	0.339±50	5.20±12	1818±31

*a, unzoned or weakly zoned cores; b, zoned rims; c, structureless rims; d, highly luminescent, nebulously-zoned grains.

**corrected for ^{204}Pb. % f^{206}Pb, common ^{206}Pb as a percentage of total ^{206}Pb.

a weighted mean ^{207}Pb/^{206}Pb age of 2077 ± 13 Ma (fig. 11A), interpreted as the age of magmatic crystallization; whereas five of seven analyses on the nebulously-zoned grains and structureless rims define another concordant population with a weighted mean ^{207}Pb/^{206}Pb age of 1826 ± 12 Ma (fig. 11A), interpreted as the age of metamorphism. Two analyses on the structureless rims (Mz-12 and Mz-16) are slightly discordant and define ages of 1882 ± 18 (1σ) Ma and 1892 ± 21 (1σ) Ma, respectively (fig. 11A), notably older than the concordant age of 1826 ± 18 Ma defined by other structureless single grains and rims. An interpretation is that these two analyses were not well positioned on the narrow recrystallization rims and overlap with some part of the zoned cores of magmatic origin.

The SHRIMP data for the granodioritic gneiss sample FP204 are included in table 9. Of 19 analyses, six were positioned on the unzoned or weakly zoned cores of types (1) and (2) zircons, three on the zoned rims of type (2) zircons, seven on the unzoned rims of type (1) zircons, and three on the nebulously-zoned grains of type (3). On a U versus Th plot (fig. 5F), the nebulously-zoned grains and structureless rims are distinctly lower in Th but markedly higher in U than those of unzoned or weakly zoned cores or zoned rims. On a concordia plot, nine analyses on the unzoned or weakly zoned cores of types (1) and (2) zircons and the zoned rims of type (2) zircons define a somewhat scattered, nearly concordant population with a weighted mean ^{207}Pb/^{206}Pb age of 2024 ± 21 Ma (fig. 11B). This age is considered to approximate the protolithic crystallization age of the granodioritic gneiss. The scatter of some analysis points (grains Gd 10, 11, and 16) may have resulted from disturbance by the later metamor-

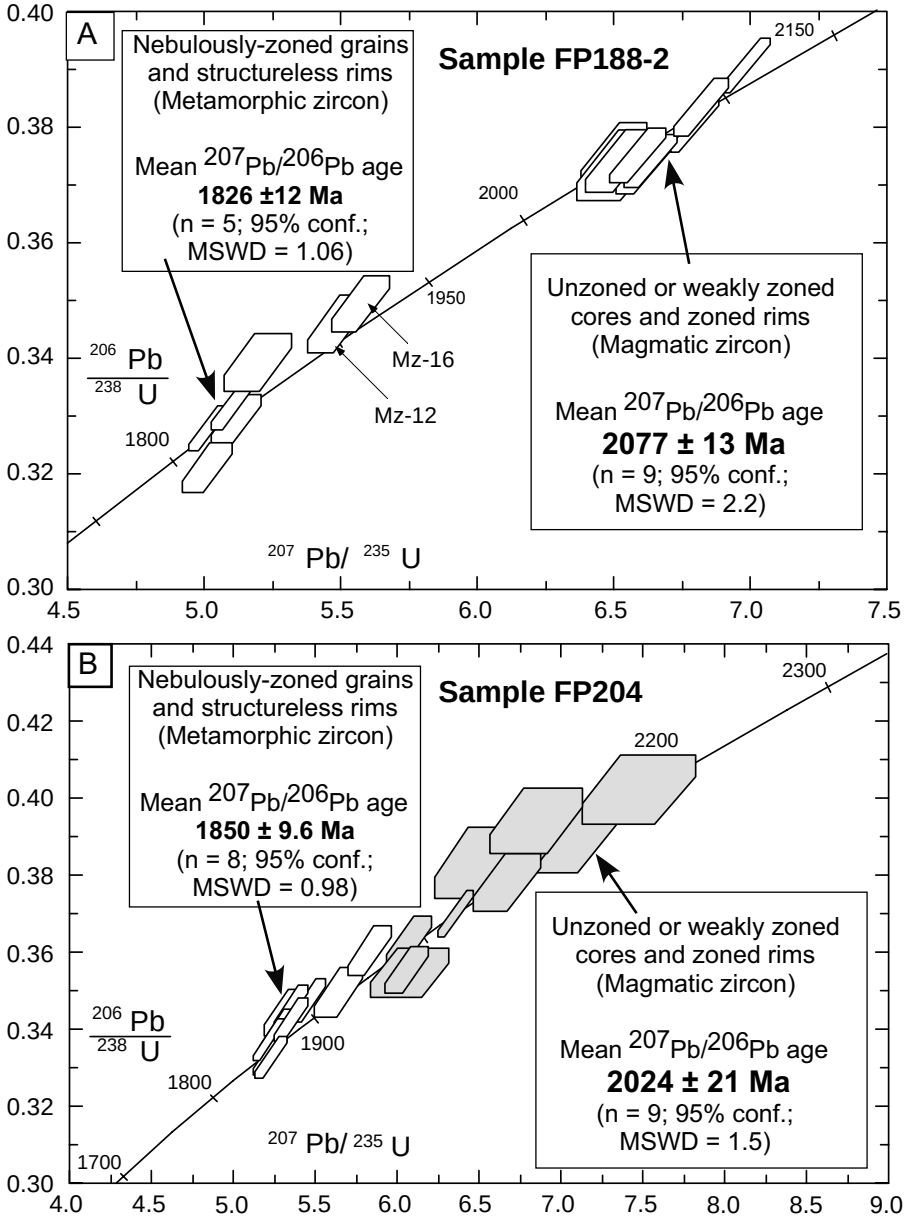

Fig. 11. Concordia plots of SHRIMP U-Pb zircon analytical results for the Nanying gneisses of the Fuping Complex. (A) Monzogranitic gneiss (sample FP 188-2); (B) Granodioritic gneiss (sample FP204).

phic event or poor positioning with some overlap with metamorphically recrystallized parts of the crystals. Eight of ten analyses on the metamorphic zircons (nebulously-zoned grains and structureless rims) form a single, well-defined, concordant or slightly discordant, and statistically-coherent population with a weighted mean $^{207}Pb/^{206}Pb$ age of 1850 ± 9.6 Ma (fig. 11B). As in sample FP188-2, this age is interpreted as the age of metamorphic recrystallization or overgrowth of zircons. Two analyses on the

TABLE 9

U–Th–Pb SHRIMP data (with 1σ errors) for granodioritic gneiss sample FP204

Grain Spot	Tex-ture*	U ppm	Th ppm	U/Th	^{204}Pb ppm	% f ^{206}Pb	^{207}Pb/^{206}Pb **	^{206}Pb/^{238}U **	^{207}Pb/^{235}U **	^{207}Pb/^{206}Pb ** Age (Ma)
Gd-1	a	37	34	0.94	17	0.47	0.131±46	0.390±92	7.04±32	2112±62
Gd-2	a	26	26	0.97	13	0.02	0.135±56	0.402±106	7.51±39	2170±72
Gd-3	a	31	17	0.56	13	1.42	0.124±58	0.383±99	6.56±37	2016±83
Gd-4	a	66	54	0.81	30	0.68	0.128±27	0.378±76	6.68±20	2072±37
Gd-5	a	32	25	0.79	15	0.99	0.125±44	0.395±95	6.83±31	2035±63
Gd-12	a	440	17	0.04	159	0.06	0.125±7	0.370±59	6.36±11	2026±9
Gd-10	b	227	45	0.20	84	0.70	0.124±16	0.355±59	6.07±13	2012±23
Gd-11	b	158	51	0.32	61	0.44	0.122±16	0.363±63	6.08±14	1979±23
Gd-16	b	54	43	0.81	23	1.79	0.125±42	0.353±74	6.10±26	2032±59
Gd-6	c	105	17	0.17	37	0.59	0.117±20	0.349±65	5.65±15	1914±31
Gd-7	c	270	3	0.01	90	0.04	0.114±9	0.347±57	5.46±10	1867±15
Gd-8	c	225	5	0.02	75	0.10	0.112±9	0.345±58	5.35±10	1839±14
Gd-9	c	136	24	0.18	50	0.32	0.118±15	0.360±64	5.84±13	1919±23
Gd-13	c	330	7	0.02	108	0.16	0.113±8	0.340±55	5.27±10	1840±12
Gd-14	c	331	4	0.01	107	0.26	0.114±9	0.333±54	5.23±10	1862±15
Gd-15	c	443	6	0.01	144	0.12	0.112±6	0.337±54	5.22±9	1837±10
Gd-17	d	321	8	0.03	103	0.04	0.114±9	0.332±54	5.24±10	1868±14
Gd-18	d	121	13	0.11	42	0.69	0.113±19	0.344±62	5.35±14	1846±30
Gd-19	d	264	6	0.02	87	0.21	0.114±9	0.342±56	5.36±10	1858±15

*a, unzoned or weakly zoned cores; b, zoned rims; c, structureless rims; d, highly luminescent, nebulously-zoned grains.

**corrected for ^{204}Pb. % f^{206}Pb, common ^{206}Pb as a percentage of total ^{206}Pb.

structureless rims are slightly reversely discordant, with older ages than the concordant age defined by analyses of other unzoned rims and structureless grains. This discordance in age can also be explained by overlap of these analyses onto some part of the zoned cores of magmatic origin.

DISCUSSION

SHRIMP U–Pb zircon geochronological data reported in this study and those presented by Wilde and others (1997) and Guan (2000), in conjunction with some Sm–Nd whole rock isochron ages and single grain evaporation zircon U–Pb ages recently determined by Liu and others (2000), enable us to place tight constraints on the timing of formation and metamorphism of the major lithologies in the Fuping Complex (table 10).

The oldest rocks in the Fuping Complex.—Both field relationships and isotopic data indicate that the known oldest components in the Fuping region are mafic granulites, amphibolites and hornblende gneisses which occur as enclaves of varying sizes in the Fuping gneisses and the Longquanguan augen gneisses. A hornblende gneiss in the Fuping gneisses was dated by Guan (2000) using SHRIMP at 2708 ± 8 Ma, which was interpreted as the crystallization age of the tonalitic protolith. Sm–Nd isotopic analyses of amphibolite and mafic granulite enclaves in the Fuping gneisses yielded a whole-

TABLE 10

Key geochronological data for the main lithologies in the Fuping Complex

Rock Assemblages	Lithologies	Rock-Forming Ages (Ma)*	Metamorphic Ages (Ma)	Sources
Pre-TTG crust	Hornblende gneisses	2708 ± 8 (a)		Guan (2000)
	Amphibolites and mafic granulites	2679 ± 69 (b)		Liu and others (2000)
Fuping TTG gneisses	Tonalitic gneiss	2523 ± 14 (a)	1802 ± 43 (a)	This study
	Trondhjemitic gneiss	2499 ± 9.5 (a)	1875 ± 43 (a)	This study
	Granodioritic gneiss	2486 ± 8 (a)	1825 ± 12 (a)	This study
	TTG gneisses	2502 ± 50 (b)		Liu and others (2000)
Longquanguan angen gneisses	Granodioritic gneiss	2540 ± 18 (a)		Wilde and others (1998)
		2543 ± 7 (a)		
	Monzongranitic gneiss	2510 ± 22 (a)		This study
	Granitic pegmatite	2507 ± 11 (a)		This study
Wanzi supracrustals	Sillimanite leptynite	<2507 ± 14 (a)		This study
	Sillimanite leptynite	<2502 ± 5 (a) Most probably <2109 ± 5		This study
Nanying gneisses	Monzongranitic gneiss	2077 ± 13 (a)	1826 ± 12 (a)	This study
	Granodioritic gneiss	2024 ± 21 (a)	1850 ± 9.6 (a)	This study
	Granitoid gneisses	2123 ± 55 (b)		Liu and others (2000)
Pegmatites	Granitic pegmatite dike		1790 ± 8 (a)	Wilde and others (1998)
	Granitic pegmatite dike		1799 ± 7 (c)	Liu and others (2000)

*(a), SHRIMP zircon U–Pb age; (b), Sm–Nd whole rock isochron age; (c), single grain evaporation zircon U–Pb age.

rock isochron age of 2679 ± 69 Ma (MSWD = 1.59), which was interpreted as the protolith age of amphibolites and mafic granulites (Liu and others, 2000). These data indicate the existence of ~2.7 Ga crustal materials in the Fuping region, which are considered to be fragments of older continental crust (Liu and others, 1985; Bai, 1986; Tian and others, 1992; Zhang, Wu, and Ye, 1991).

Late Archean to Early Paleoproterozoic granitoid magmatism.—One of the key issues concerns the age of the Fuping tonalitic-trondhjemitic-granodioritic gneisses that make up over 60 percent of the total exposure of the complex. An early suggestion, based on a conventional multigrain zircon U–Pb study by Liu and others (1985), that the main period of formation of the Fuping gneisses was between 2800 and 2560 Ma was contested by Sun, Armstrong, and Lambert (1992) whose Nd isotopic studies suggested that there was no significant amount of continental crust older than 2.6 Ga in the Fuping region. The latter view is supported by our present SHRIMP data that constrain the period of emplacement of the Fuping gneisses between 2520 and 2480 Ma. Whereas Pb-loss and new zircon growth during metamorphism have altered the U–Pb system in the zircons, U–Pb analyses on the magmatic zircons reveal that the first

major phase of the Fuping gneisses was the emplacement of tonalites at 2523 ± 14 Ma, followed by the emplacement of trondhjemites at 2499 ± 9.5 Ma and intrusion of granodiorites at 2486 ± 8 Ma. Therefore, our data do not support the original suggestion by Liu and others (1985) that the major crustal accretion of the Fuping region occurred before 2560 Ma. Most recently, Liu and others (2000) obtained a Sm–Nd whole rock isochron age of 2502 ± 50 Ma (MSWD = 1.4) from six compositionally different Fuping gneiss samples. Although this age cannot be used to constrain the precise time of emplacement of the Fuping gneisses, it supports our conclusion that the major crustal accretion of the Fuping region occurred between 2520 and 2480 Ma.

Another question related to the main granitoid magmatism in the Fuping Complex concerns the timing of the Longquanguan augen gneisses and their geological relationship with the Fuping gneisses. The Longquanguan augen gneisses were previously treated as the youngest lithological unit in the Fuping Complex and were considered to unconformably overlie other lithologies of the complex (Ren, 1980), largely based on the fact that the regional foliation of other lithologies in the Fuping Complex is truncated by the gneissosity of the Longquanguan augen gneisses (fig. 3), and that the Longquanguan augen gneisses are lower in metamorphic grade than some other lithologies in the complex. However, this argument has been challenged by Li and Qian (1991) who recognized that the Longquanguan augen gneisses are mainly exposed along a large scale ductile shear zone, named the Longquanguan–Yulinping shear zone, and proposed that the augen gneisses were the mylonitized products of the Fuping gneisses. This is partly supported by Wilde and others (1998) who dated two Longquanguan augen gneiss samples at 2540 ± 18 Ma and 2543 ± 7 Ma, using the SHRIMP technique. These data and our present SHRIMP ages (table 5) indicate that the augen gneisses along the Longquanguan–Yulinping shear zone are not younger, but slightly older, than the Fuping gneisses, whereas the augen gneisses along the Ciyu–Xinzhuang shear zone, dated in this paper at 2510–2507 Ma, are similar in age to the Fuping tonalitic and trondhjemitic gneisses. These results show that the augen gneisses along the two ductile shear zones do not have the same crystallization age; the augen gneisses along the Longquanguan–Yulinping shear zone may have been derived from the relatively older and possibly deeper-seated gneisses which were mylonitized and exhumed along the shear zone.

Wanzi supracrustal assemblage: Archean or Paleoproterozoic?—Like the Fuping gneisses, the Wanzi supracrustal assemblage in the Fuping Complex is also considered to have been deposited between 2800 and 2560 Ma, constrained by the conventional multigrain zircon U–Pb ages reported by Liu and others (1985) and Wu and others (1989). However, SHRIMP U–Pb zircon data of the present study do not support this result. The morphologies and internal structures of zircons from two high-grade metasedimentary supracrustal rock samples (FP249 and Fp260) dated in this study support a detrital origin from an igneous source, although most have been rounded by subsequent sedimentary processes. The cores of zircons from the sillimanite-bearing gneiss sample FP249 and the sillimanite-bearing leptynite sample FP260 have mean $^{207}Pb/^{206}Pb$ ages of 2502 ± 7 Ma and 2507 ± 14 Ma (fig. 10A, B), respectively. These ages cannot be interpreted as the timing of metamorphism because no overgrowth or recrystallization in these zircon cores has been revealed by CL images, and the cores do not have low Th/U ratios suggestive of metamorphic growth (Williams and Claesson, 1987; Pidgeon, Macambira, and Lafon, 2000). These ages most likely represent the crystallization ages of igneous source rocks which contributed to these sedimentary supracrustal rocks. Therefore, these rocks must have been deposited no earlier than ~2507 my ago. In addition, sample FP249 contains a zoned zircon grain (Sg-19) with a near concordant age of 2109 ± 5 Ma (1σ). If this age provides a maximum depositional age for this rock, the pelitic rocks in the Wanzi supracrustal assemblage must have been

deposited after ~2110 Ma. This conclusion is supported by Guan (2000) who has obtained a SHRIMP U–Pb zircon age of 2097 ± 46 Ma from the fine-grained paragneiss of the Wanzi supracrustals. Whether or not all rocks in the Wanzi supracrustal assemblage formed in the Paleoproterozoic remains unknown because of a lack of isotopic data for other rocks in the supracrustal series. It should be noted that a few zircon cores from samples FP249 and FP260 yielded older ages in the range 2550 to 2800 Ma, but the features of these zircon cores (fig. 9A) suggest a xenocrystic origin, and thus these ages cannot be used to constrain the timing of deposition of the rocks.

Paleoproterozoic granitic magmatism.—The last major phase of granitoid formation in the Fuping Complex was the emplacement of the Nanying granitic gneisses, which have been mapped out recently by Liu and others (2000) and Zhao and others (2000a). The Nanying granitic gneisses consist predominantly of monzogranitic and granodioritic gneisses, which are clearly intrusive into the Fuping gneisses. The petrogenesis of these gneisses is interpreted to result from partial melting of the Fuping gneisses or other older lithologies in the Fuping Complex (Liu and others, 2000). SHRIMP results presented in this study indicate that granitic magmatism assigned to the Nanying granitic gneisses do not have the same age, although they display similar fabrics and intrusive relationship with the tonalitic-trondhjemitic-granodioritic gneisses. The monzogranitic rocks were emplaced at 2077 ± 13 Ma ago, somewhat earlier than the emplacement of the granodioritic rocks, which was dated at 2024 ± 21 Ma. Most recently, Liu and others (2000) obtained a Sm–Nd whole rock isochron age of 2123 ± 55 Ma (MSWD = 1.22) from seven Nanying gneiss samples, and interpreted it as their average crystallization age.

Age of regional metamorphism of the Fuping Complex: Late Archean or Paleoproterozoic?—In Chinese geological literature, the term 'Fuping Orogeny' has long been used for a ~2.5 Ga geological event that resulted in widespread deformation and regional metamorphism of 2.8–2.5 Ga and older Archean terrains, including the Fuping Complex, in the North China Craton (Ren, 1980; Wu and others, 1989; Tian, 1991; Bai and Dai, 1998). Accordingly, it has been taken for granted by some Chinese geologists that the regional metamorphism of the Fuping Complex occurred at ~2.5 Ga (Liu and others, 1985; Wu and others, 1989; Tian, 1991). This conclusion is based on the view that the U–Pb system in zircon can be completely reset during high-grade metamorphism, and that the zircon data of ~2.5 Ga throughout these Archean terrains reflect the age of regional metamorphism. However, numerous studies have shown that zircons can survive high-grade regional metamorphism without losing their age information (Hölzl and others, 1994; Kröner, Jaeckel, and Williams, 1994). Mezger and Krogstad (1997) suggest that complete resetting of U–Pb systems in zircon under crustal conditions is only possible through dissolution of pristine zircons and reprecipitation to form new single grains or overgrowth rims, whereas partial resetting results mainly from recrystallization of metamict domains of zircons.

The present study confirms the existence of metamorphic zircons in nearly all medium- to high-grade lithologies from the Fuping Complex, based on zircon internal structures illustrated by CL images and their U–Th contents. These metamorphic zircons occur as either single nebulously-zoned grains or overgrowth/recrystallization rims surrounding magmatic zircon cores, and are all characterized by extremely high luminescence (figs. 4 and 9) and very low Th contents (fig. 5). These features make them distinctly different from the pristine magmatic zircons, which are generally characterized by oscillatory zoning, low luminescence (figs. 4 and 9) and comparatively high Th and U contents (fig. 5). Although overgrowth or recrystallization rims in the Longquanguan augen gneisses and the Wanzi supracrustal rocks are too narrow to be analyzed, the nebulously-zoned grains and structureless rims from the Fuping gneisses and the Nanying granitic gneisses yield similar concordant $^{207}Pb/^{206}Pb$ ages in the

range ~1875 to 1802 Ma, which are 600–700 Ma and 150–250 Ma younger than the magmatic crystallization ages of the Fuping gneisses and the Nanying granitic gneisses, respectively. We believe that the ages of 1875–1802 Ma of these nebulously-zoned grains and structureless rims approximate the age of regional metamorphism of the Fuping Complex. This conclusion is supported by the SHRIMP U–Pb zircon age of 1790 Ma obtained by Wilde and others (1998) and a $^{207}Pb/^{206}Pb$ zircon age (evaporation technique) of 1799 Ma by Liu and others (2000) from syntectonic pegmatite dikes in the Fuping Complex (table 10). It should be noted that some weakly zoned zircon rims from the Fuping gneisses yielded a concordant to discordant group with an age of 2330–2380 Ma. One explanation for this age group is the existence of an earlier metamorphic event. This question is not pursued here. Our conclusion from these data is that the regional metamorphism of the Fuping Complex occurred in the late Paleoproterozoic, not at the end of the Archean, as previously considered by most Chinese geologists.

Comparison with the Wutai and Hengshan Complexes and Tectonic Implications

New SHRIMP zircon U–Pb ages presented in this study (table 10) for the Fuping Complex are comparable to recent U–Pb zircon ion probe results reported by Wilde and others (1997, 1998, unpublished data) for the Wutai and Hengshan Complexes (table 11). As shown in tables 10 and 11, lithological and geochronological data for the Fuping, Hengshan and Wutai Complexes indicate that they are characterized by the emplacement of major granitoid bodies at around 2.52 Ga to 2.48 Ga ago, deposition of supracrustal rocks most probably in the Paleoproterozoic, intrusion of granitic bodies at ~2.1–2.0 Ga, and regional metamorphism at ~1.875–1.802 Ga. Geochemical data from these complexes suggest that they formed in a supra-subduction zone setting (Wilde and others, 1997, 1998). They also indicate that the high-grade Fuping and Hengshan Complexes do not represent an older crystalline basement to the low-grade Wutai Complex, as suggested in many previous tectonic models (Bai, 1986; Li and others, 1990; Tian, 1991; Bai and others, 1992; Yuan and Zhang, 1993; Wang and others, 1996). Thus, the tectonic evolution of the Fuping Complex may not be related to local interaction of the Wutai, Fuping and Hengshan Complexes, either through closure of an intracratonic rift (Tian, 1991; Yuan and Zhang, 1993) or a large oceanic tract (Bai, 1986; Bai and others, 1992; Li and others, 1990; Wang and others, 1996). We consider that the three complexes all represent elements of a single late Archean to Paleoproterozoic magmatic arc system that has been subsequently tectonically disrupted and juxtaposed to the North China Craton at around 1.85 Ga.

As discussed earlier, an extensive lithological, structural, metamorphic, geochemical and geochronological analysis of the North China Craton has suggested that the craton can be divided into the Eastern and Western Blocks, separated by the Central Zone (fig. 12; Zhao and others, 2000b, 2001a). The Eastern Block, including Southern Anshan–Benxi, Eastern Hebei, Southern Jilin, Northern Liaoning, Southern Liaoning, Western Liaoning, Miyun, Western Shandong, Eastern Shandong Complexes (fig. 12), consists predominantly of late Archean domiform tonalitic–trondhjemitic–granodioritic batholiths outlined by anastomosing networks and linear belts of open to tight synforms of minor volcanic and sedimentary rocks metamorphosed from greenschist to granulite facies at ~2.5 Ga, with anticlockwise P–T paths involving near-isobaric cooling, which reflect an origin related to underplating and intrusion of mantle-derived magmas (Zhao and others, 1998, 2001a). Some early to middle Archean rocks are locally present in the Eastern Block (Liu and others, 1992; Song and others, 1996), but their tectonic history is unclear due to reworking by the 2.5 Ga tectonothermal event. The Western Block, including the Helanshan-Qianlishan, Daqing–Ulashan, Guyang–Wuchuan, Sheerteng and Jining Complexes (fig. 12), has a late Archean lithological assemblage, structural style and metamorphic history similar to that of the

TABLE 11

SHRIMP U–Pb zircon ages of the Hengshan and Wutai Complexes

Rocks	Localities	$^{207}Pb/^{206}Pb$	Interpretations	References
Hengshan Complex				
Tonalitic gneiss	Tashikou	2520 ± 15*	Crystallization age	Wilde, unpubl data
		1872 ± 17**	Metamorphic age	
Tonalitic gneiss	Yixingzhai	2499 ± 4	Crystallization age	Wilde, unpubl data
Garnet quartzite	Yanmenguan	2527 ± 10*	Age of source rocks	Wilde, unpubl data
		1872 ± 17**	Metamorphic age	
Mafic granulite	Dashihe	1827 ± 10	Metamorphic age	Wilde, unpubl data
Wutai Complex				
Granitic gneiss	Erkou	2566 ± 13	Crystallization age	Wilde et al. (1997)
Granitic gneiss	Erkou	2555 ± 6	Crystallization age	Wilde et al. (1997)
Augen gneiss	Lanzhishan	2553 ± 8	Crystallization age	Wilde et al. (1997)
Granitic gneiss	Chechang-Beitai	2552 ± 5	Crystallization age	Wilde et al. (1997)
Granitic gneiss	Chechang-Beitai	2546 ± 3	Crystallization age	Wilde et al. (1997)
Granitic gneiss	Chechang-Beitai	2542 ± 7	Crystallization age	Wilde et al. (1997)
Granitic gneiss	Chechang-Beitai	2538 ± 6	Crystallization age	Wilde et al. (1997)
Granitic gneiss	Hongyachun	2537 ± 10	Crystallization age	Wilde et al. (1997)
Granitic gneiss	Guangmingsi	2531 ± 5	Crystallization age	Wilde et al. (1997)
Granitic gneiss	Shifo	2531 ± 4	Crystallization age	Wilde et al. (1997)
Granitic gneiss	Wangjiahui	2520 ± 9	Crystallization age	Wilde et al. (1997)
Granitic gneiss	Wangjiahui	2517 ± 12	Crystallization age	Wilde et al. (1997)
Greenschist	Taihuai-Shahe	2555 ± 12	Protolith age	Wilde et al. (1997)
Meta-andesite	Taihuai-Shahe	2533 ± 8	Protolith age	Wilde et al. (1997)
Metadacite	Taihuai-Shahe	2524 ± 8	Protolith age	Wilde et al. (1997)
Rhyodacite	Taihuai-Shahe	2523 ± 18	Protolith age	Wilde et al. (1997)
Subvolcanics	Taihuai-Shahe	2516 ± 8	Protolith age	Wilde et al. (1997)
Monzogranite	Wangjiahui	2117 ± 18	Crystallization age	Wilde et al. (1997)
Porphyric granite	Dawaliang	2176 ± 12	Crystallization age	Wilde et al. (1997)
Porphyric granite	Dawaliang	2107 ± 15	Crystallization age	Wilde et al. (1997)

*Age of group 1; **age of group 2.

Eastern Block, but differs in the absence of early to middle Archean assemblages and in being overlain by, and interleaved with, Paleoproterozoic khondalites which were affected by a ~1.85 Ga metamorphic event involving clockwise P-T paths (Jin, Li, and Liu, 1991; Lu, 1991; Lu and Jin, 1993; Lu, Xu, and Liu, 1996; Wu and Zhong, 1998; Wu and others, 2000).

The Fuping, Wutai and Hengshan Complexes, along with the Dengfeng, Huaian, Lüliang, Northern Hebei, Taihua, Zanghuang and Zhongtiao Complexes, lie in the Central Zone that is bounded by two major fault systems (fig. 12). The orogen consists of late Archean to Paleoproterozoic tonalitic-trondhjemitic-granodioritic gneisses, interleaved with abundant sedimentary and volcanic rocks that are interpreted as having developed in magmatic arc and intra-arc basin environments from their geochemistry (Bai, 1986; Wu and others, 1989; Sun, Armstrong, and Lambert, 1992; Wang and others, 1996; Zhao, Cawood, and Lu, 1999; Zhao and others, 2000a, b). These rocks underwent multiple phases of compressional deformation and peak medium- to high-pressure metamorphism followed by rapid erosion and exhumation,

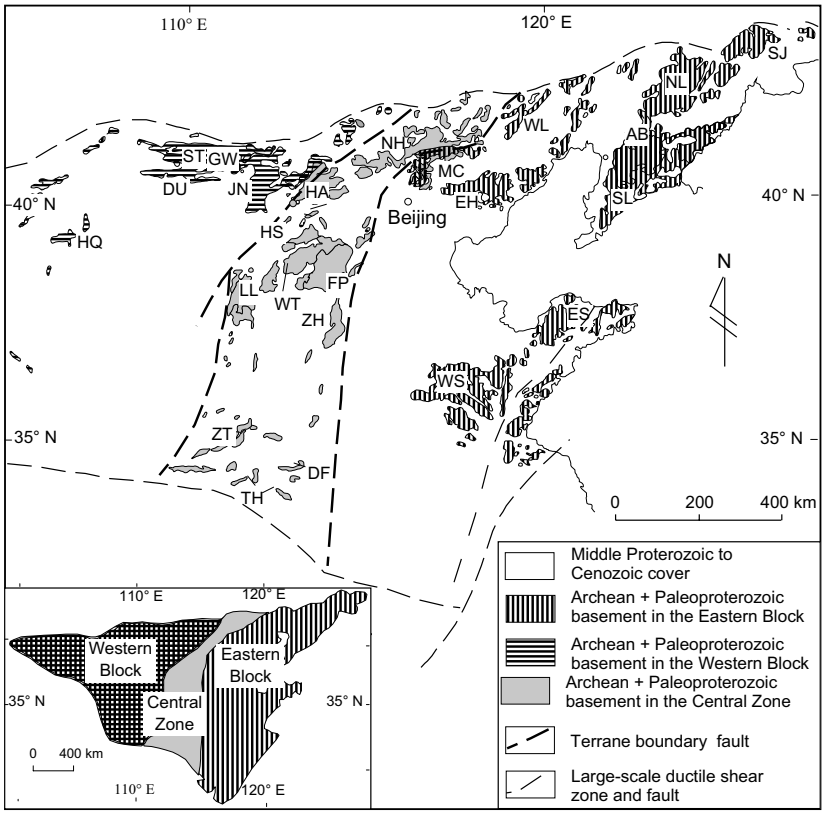

Fig. 12. Distribution of basement rocks in the North China Craton and the relationship of the Eastern and Western Blocks to the Central Zone (Inset). The Eastern Block includes the Anshan-Benxi (AB), Eastern Hebei (EH), Eastern Shandong (ES), Miyun (M), Northern Liaoning (NL), Southern Jilin (SJ), Southern Liaoning (SL), Western Liaoning (WL) and Western Shandong (WS) Complexes; the Western Block includes the Daqingshan-Ulashan (DU), Guyang-Wuchuan (GW), Helanshan-Qianlishan (HQ), Jinning (JN) and Sheerteng (ST) Complexes; the Trans-North China Orogen includes the Dengfeng (DF), Fuping (FP), Hengshan (HS), Huaian (HA), Lüliang (LL), Northern Hebei (NH), Taihua (TH), Wutai (WT), Zanghuang (ZH) and Zhongtiao (ZT) Complexes.

reflecting a continental collisional environment (Li and others, 1990; Zhai and others, 1992; Wang and others, 1996; Wu and Zhong, 1998; Zhao and others, 2000a, b). Based on new SHRIMP results presented in this paper and our previous petrological, geochemical and metamorphic P–T–t path studies (Zhao and others, 1998, 1999a, 2000a, b), it is proposed that in the late Archean, the Eastern and Western Blocks existed as two separate Archean continental blocks that developed through the intrusion and underplating of mantle magmas, whereas the Central Zone represents a late Archean to Paleoproterozoic continental magmatic arc, which was deformed and metamorphosed during collision between the Eastern and Western Blocks at ~1.85 Ga, resulting in the final assembly of the North China Craton.

ACKNOWLEDGMENTS

We thank R. T. Pidgeon for reviewing an earlier version of this paper. The final version of the paper has benefited from the perceptive comments of journal reviewers R. Tucker and T. Kusky and the Editor J. J. Ague. The work was supported by an ARC Large Grant (A39532446) to S. A. Wilde and P. A. Cawood and RGC Grants (HKU7300/

99P and HKU7115/00P) to M. Sun. This work is Tectonics Special Research Centre Publication No. 152.

Appendix A. Sample Description

The Fuping gneiss sample FG1 is a banded hornblende-biotite-plagioclase tonalitic gneiss (plagioclase 60%, quartz 20%, biotite 10% and hornblende <5% with accessory apatite, titanite, opaque oxide and zircon). The sample is medium grained and strongly banded with the development of continuous layers of plagioclase and quartz aggregates. Both biotite and hornblende show some alignment in the foliation. Sample FP217 is a banded hornblende-biotite-plagioclase trondhjemitic gneiss, with mineralogy and fabrics similar to sample FG1, but its plagioclase is dominated by oligoclase. The third Fuping gneiss sample FP216 is a fine-grained biotite granodioritic gneiss (plagioclase 40%, quartz 20%, K-feldspar 20%, biotite >15%, with accessory allanite, apatite, titanite, opaque oxide and zircon). Most biotite flakes in the sample are oriented to form a distinct foliation, but some larger flakes occur as aggregates which are surrounded by symplectites of felsic phases + allanite + opaque oxide. The Wanzi supracrustal rock sample FP249 is a fine-to medium-grained sillimanite-bearing gneiss (quartz 35%, K-feldspar 30%, plagioclase 25%, biotite 5%, sillimanite <5%, with accessory apatite, titanite, opaque oxide and zircon). Fibrous sillimanite occurs with quartz grains as ball-shaped aggregates ranging between 1 and 10 cm in diameter. Another supracrustal rock sample FP260 is similar in mineralogy and fabrics to sample FP249, but its feldspar is composed exclusively of K-feldspar (>50%) and the modal content of biotite increases up to 10%. Both of the two Longquanguan augen gneiss samples (FP236 and FP224) were collected from the Ciyu–Xinzhuang ductile shear zone since the augen gneisses along the Longquanguan–Yulinping ductile shear zone have been dated by Wilde and others (1997). Sample FP236 is a relatively weakly deformed monzogranitic augen gneiss, which was taken at a locality about 8 km west of Ciyu Village (fig. 3). It comprises plagioclase (35%), K-feldspar (25%), quartz (25%), and biotite (<15%), with accessory monazite, apatite, titanite, opaque oxide and zircon. Biotites are intensely aligned into a strong foliation. K-feldspars occur as megacrysts that have been deformed (mylonitized) to form augens. Sample FP224 is a weakly mylonitized pegmatite dike about 2-m-wide cutting the augen gneiss (sample FP236) and comprises coarse-grained K-feldspar (50%), quartz (30%), plagioclase (10%) and biotite (10%). The dike shows a strong foliation defined by the oriented biotite flakes and elongated quartz grains, which is parallel to the foliation of the host augen gneiss. Samples FP188-2 and FP204 were collected from the Nanying granitic gneisses which intrude the Fuping gneisses. Sample FP188-2 is monzogranitic in composition (plagioclase 35%, K-feldspar 30%, quartz 25%, biotite 5% and hornblende <5%), whereas sample FP204 is granodioritic (plagioclase 50%, quartz 25%, K-feldspar 15%, biotite 5%, hornblende <5%). Both samples are fine- to medium-grained and show a weak foliation defined by oriented biotite and hornblende.

References

Ashwal, L. D., Tucker, R. D., and Zinner, E. K., 1999, Slow cooling of deep crustal granulites and Pb-loss in zircon: Geochimica et Cosmochimica Acta, v. 63, p. 2839–2851.

Bai, J., 1986, The Precambrian crustal evolution of the Wutaishan area, *in* Bai, J., editor, The Early Precambrian Geology of Wutaishan: Tianjin, Tianjin Science and Technology Press, p. 376–383 (in Chinese).

Bai, J., and Dai, F. Y., 1998, Archean crust of China, *in* Ma, X. Y., and Bai, J., editors, Precambrian crust evolution of China: Beijing, Springer-Geological Publishing House, p. 15–86.

Bai, J., Wang, R. Z., and Guo, J. J., 1992, The Major Geologic Events of Early Precambrian and Their Dating in Wutaishan Region: Beijing, Geological Publishing House, 63 p.

Bodorkos, S., Cawood, P. A., Oliver, N. H. S., and Nemchin, A., 2000, Rapidity of orogenesis in the Paleoproterozoic Halls Creek Orogen, northern Australia: evidence from SHRIMP zircon data, CL zircon images, and mixture modeling studies: American Journal of Science, v. 300, p. 60–80.

Compston, W., Williams, I. S., and Meyer, C., 1984, U–Pb geochronology of zircons from Lunar breccia 73217 using a sensitive high mass-resolution ion microprobe: Journal of Geophysical Research, v. 89B, p. 525–534.

Guan, H., ms, 2000, The Fuping Complex and its significance in early Precambrian crustal evolution of Sino-Korean Craton: Ph.D. thesis, The University of Hong Kong, Hong Kong, 223 p.

Guo, J. H., and Zhai, M. G., 2001, Sm-Nd age dating of high-pressure granulites and amphibolites from Sanggan area, North China Craton: Chinese Science Bulletin, v. 46, p. 106–111.

Guo, J. H., Zhai, M. G., and Zhang, Y. G., 1993, Early Precambrian Manjinggou high-pressure granulites melange belt on the southern edge of the Huaian Complex, North China Craton: geological features, petrology and isotopic geochronology: Acta Petrologica Sinica, v. 9, p. 329–341 (in Chinese with English abstract).

Guo, J. H., Zhai, M. G., Li, Y. G., and Yan, Y. H., 1998, Contrasting metamorphic P-T paths of Archean

high-pressure granulites from the North China Craton: metamorphism and tectonic significance: Acta Petrologica and Sinica, v. 14, p. 430–448.
Guo, J. H., Zhai, M. G., Li, Y. G., and Li, J. H., 1999, Metamorphism, PT paths and tectonic significance of garnet amphibolites and granulites from Hengshan, North China Craton: Scientia Geologica Sinica, v. 34, p. 311–325.
Guo, J. H., Wang, S. S., Sang, H. Q., and Zhai, M. G., 2001, $^{40}Ar/^{39}Ar$ age spectra of garnet porphyroblast: implications for metamorphic age of high-pressure granulite in the North China Craton: Acta Petrologica Sinica, v. 17, p. 436–442.
Hanchar, J. M., and Miller, C. F., 1993, Zircon zonation patterns as revealed by cathodoluminescence and backscattered electron images: implications for interpretation of complex crustal histories: Chemical Geology, v. 110, p. 1–13.
Hanchar, J. M., and Rundnick, R. L., 1995, Revealing hidden structures: The application of cathodoluminescence and back-scattered electron imaging to dating zircons from lower crustal xenoliths: Lithos, v. 36, p. 289–303.
He, G. P., and Ye, H. W., 1998, Two types of Metamorphism of Paleoproterozoic basement in Eastern Liaoning and Southern Jilin area: Acta Petrologica Sinica, v. 14, v. 152–162.
Hölzl, S., Hofmann, A. W., Todt, W., and Köhler, H., 1994, U–Pb geochronology of the Sri Lankan basement: Precambrian Research, v. 66, p. 123–149.
Huang, J. Q., 1977, Basic outline of China tectonics: Acta Geologica Sinica, v. 52, p. 117–135 (in Chinese).
Huang, X., Bai, Z., and DePaolo, D. J., 1986, Sm-Nd isotope study of early Archaean rocks, Qianan, Hebei Province, China: Geochimica et Cosmochimica Acta, v. 50, p. 625–631.
Jahn, B. M., and Zhang, Z. Q., 1984, Archean granulite gneisses from eastern Hebei Province, China: rare earth geochemistry and tectonic implications: Contributions to Mineralogy and Petrology, v. 85, p. 224–243.
Jahn, B. M., Auvray, B., Cornichet, J., Bai, Y. D., Shen, Q. H., and Liu, D. Y., 1987, 3.5 Ga old amphibolites from eastern Hebei Province, China: field occurrence, petrography, Sm–Nd isochron age and REE geochemistry: Precambrian Research, v. 34, p. 311–346.
Jin, W., Li, S. X., and Liu, X. S., 1991, Metamorphic dynamics of Early Precambrian high-grade metamorphic rocks in Daqingshan-Ulashan area, Inner Mongolia: Acta Petrologica Sinica, v. 7, p. 27–25.
Kennedy, A. K., and de Laeter, J. R., 1994, The performance characteristics of the WA SHRIMP II ion microprobe: 8th International Conference on Geochronology, Cosmochronology and Isotope Geology, Berkeley, Abstracts, v. 1107, p. 166.
Kröner, A., and Jaeckel, P., 1995, Dating the peak of high-temperature regional metamorphism by using metamorphic zircons: EOS, v. 76, p. 703–704.
Kröner, A., Compston, W., Zhang, G. W., Guo, A. L., and Todt, W., 1988, Ages and tectonic setting of Late Archean greenstone-gneiss terrain in Henan Province, China, as revealed by single-grain zircon dating: Geology, v. 16, p. 211–215.
Kröner, A., Jaeckel, P., and Williams, I. S., 1994, Pb-loss patterns in zircons from a high-grade metamorphic terrain as revealed by different dating methods—U-Pb and Pb-Pb ages for igneous and metamorphic zircons from northern Sri-Lanka: Precambrian Research, v. 66, p. 151–181.
Kröner, A., Cui, W. Y., Wang, W. Y., Wang, C. Q., and Nemchin, A. A., 1998, Single zircon ages from high-grade rocks of the Jianping Complex, Liaoning Province, NE China: Journal of Asian Earth Sciences, v. 16, p. 519–532.
Kröner, A., O'Brien, P. J., Nemchin, A. A., and Pidgeon, R. T., 2000, Zircon ages for high pressure granulites from South Bohemia, Czech Republic, and their connection to Carboniferous high temperature processes: Contributions to Mineralogy and Petrology, v. 138, v. 127–142.
Li, J. H., and Qian, Q. L., 1991, A study on Longquanguan shear zone in northern part of Taihang Mountain: Shanxi Geology, v. 6, p. 17–29 (in Chinese).
Li, J. H., Kroner, A., Qian, X. L., and O'Brien, P., 2000, Textonic Evolution of an Early Precambrian High-Pressure Granulite Belt in the North China Craton: Acta Geologica Sinica, v. 74, p. 246–258.
Li, J. L., Wang, K. W., Wang, Q. C., Liu, X. H., and Zhao, Z. Y., 1990, Early Proterozoic collision mountain belt in Wutaishan area, China: Scientia Geologica Sinica, v. 25, p. 1–11 (in Chinese).
Liu, D. Y., Page, R. W., Compston, W., and Wu, J. S., 1985, U-Pb zircon geochronology of Late Archean metamorphic rocks in the Tailangshan-Wutaishan area, North China: Precambrian Research, v. 27, p. 85–109.
Liu, D. Y., Nutman, A. P., Compston, W., Wu, J. S., and Shen, Q. H., 1992, Remnants of ≥3800 Ma crust in the Chinese Part of the Sino-Korean craton: Geology, v. 20, p. 339–342.
Liu, S. W., 1997, Study on fluid-rock equilibrium system of Fuping gneiss complex, Taihang Mountains: Science in China, v. 40, p. 239–245.
Liu, S. W., and Liang, H. H., 1997, Metamorphism of Al-rich gneisses from the Fuping Complex, Taihang Mountain, China: Acta Petrologica Sinica, v. 13, p. 303–312.
Liu, S. W., Liang, H. H., and Hua, Y. G., 1999, Geochemistry and petrogenesis of sillimanite-quartz ball-bearing granites in Taihangshan region: Scientia Geologica Sinica, v. 34, p. 390–396.
Liu, S. W., Liang, H. H., Zhao, G. C., Hua, Y. G., and Jian, A. H., 2000, Isotopic chronology and geological events of Precambrian complex in Taihangshan region: Science in China, v. 43, p. 386–393.
Lu, L. Z., 1991, Metamorphic P–T–t path of the Archean granulite-facies terrains in Jining area, Inner Mongolia and its tectonic implications: Acta Petrologica Sinica, v. 8, p. 1–12.
Lu, L. Z., and Jin, S. Q., 1993, P–T–t paths and tectonic history of an early Precambrian granulite facies terrane, Jining district, southeastern Inner Mongolia, China: Journal of Metamorphic Geology, v. 11, p. 483–498.
Lu, L. Z., Xu, X. C., and Liu, F. L., 1996, Early Precambrian khondalites in North China: Changchun, Jilin Science & Technology Press, 276 p.

Ludwig, K. R., 2001, Users Manual for a geochronological toolkit for Microsoft Excel: Berkeley Geochronology Center, Special Publication No. 1a, 59 p.
Ma, X. Y., Bai, J., Shuo, S. T., Lao, Q. Y., and Zhang, J. S., 1987, The Early Precambrian tectonic framework of China and research methods: Beijing, Geological Publishing Press, 131 p. (in Chinese).
Mezger, K., and Krogstad, E. J., 1997, Interpretation of discordant U–Pb zircon ages: An evaluation: Journal of Metamorphic Geology, v. 15, p. 127–140.
Nelson, D. R., 1997, Compilation of SHRIMP U-Pb zircon geochronology data, 1996: Geological Survey of Western Australia, Record 1997/2, 189 p.
Pidgeon, R. T., 1992, Recrystallization of oscillatory zoned zircon: some geochronological and petrological implications: Contributions to Mineralogy and Petrology, v. 110, p. 463–472.
Pidgeon, R. T., and Wilde, S. A., 1998, The interpretation of complex zircon U–Pb systems in Archean granitoids and gneisses from the Jack Hills, Narryer Gneiss Terrane, Western Australia: Precambrian Research, v. 91, p. 309–332.
Pidgeon, R. T., Nemchin, A. A., and Hitchen, G. J., 1998, Internal structures of zircons from Archean granites from the Darling Range batholith: implications for zircon stability and the interpretation of zircon U–Pb ages: Contributions to Mineralogy and Petrology, v. 132, p. 288–299.
Pidgeon, R. T., Macabira, M. J. B., and Lafon, J.-M., 2000, Th–U–Pb isotopic system and internal structures of complex zircon from an enderbite from the Pium Complex, Carajás Province, Brazil: evidence for the ages of granulite facies metamorphism and the protolith of the enderbite: Chemical Geology, v. 166, p. 159–171.
Pupin, J. P., 1980, Zircon and granite petrology: Contributions to Mineralogy and Petrology, v. 73, p. 207–220.
Ren, J. S., 1980, Tectonics and evolution of China: Beijing, Science Press, 275 p. (in Chinese).
Rowley, D. B., Xue, F., Tucker, R. D., Peng, Z. X., Baker, J., and Davis, A., 1997, Ages of ultrahigh pressure metamorphism and protolith orthogneisses from the eastern Dabie Shan: U/Pb zircon geochronology: Earth and Planetary Science Letters, v. 191, p. 191–203.
Shen, Q. H., Liu, D. Y., Wang, P., and Gao, J. F., 1987, U–Pb and Rb–Sr isotopic ages of metamorphic rock series from the Jining Group, southern Inner Mongolia: Journal of China Institute of Geology, v. 16, p. 165–178 (in Chinese).
Shui, T., 1987, Tectonic framework of the southeastern China continental basement: Science in China, v. 31, p. 885–896.
Song, B., Nutman, A. P., Liu, D. Y., and Wu, J. S., 1996, 3800 to 2500 Ma crustal evolution in Anshan area of Liaoning Province, Northeastern China: Precambrian Research, v. 78, p. 79–94.
Steiger, R. H., and Jäger, E., 1977, Subcommission on geochronology: convention on the use of decay constants in geo- and cosmochronology: Earth and Planetary Science Letters, v. 36, p. 359–362.
Sun, M., Armstrong, R. L., and Lambert, R. St. J., 1992, Petrochemistry and Sr, Pb and Nd isotopic geochemistry of Early Precambrian rocks, Wutaishan and Taihangshan areas, China: Precambrian Research, v. 56, p. 1–31.
Tang, X. M., and Liu, S. W., 1997, Extensional deformation belt in the Archean metamorphic rocks in the Northern Taihang mountains: Journal of Peking University, v. 33, p. 447–455.
Tian, Y. Q., 1991, Geology and Mineralization of Wutai–Hengshan Greenstone Belt: Taiyuan, Shanxi Science and Technology Press, 244 p. (in Chinese).
Tian, Y. Q., Liang, Y. F., Fan, S. K., Zhu, B. Q., and Chen, L. W., 1992, Geochronology and Nd isotropic evolution of the Hengshan Complex: Geochimica Sinica, v. 3, p. 255–263.
Vavra, G., 1990, On the kinematics of zircon growth and its petrogenetic significance: a cathodoluminescence study: Contributions to Mineralogy and Petrology, v. 106, p. 90–99.
Vavra, G., Gebauer, D., Schmidt, R., and Compston, W., 1996, Multiple zircon growth and recrystallization during polyphase late Carboniferous to Triassic metamorphism in granulites of the Ivrea Zone (southern Alps): an ion microprobe (SHRIMP) study: Contributions to Mineralogy and Petrology, v. 122, p. 337–358.
Vavra, G., Schmidt, R., and Gebauer, D., 1999, Internal morphology, habit and U–Th–Pb microanalysis of amphibolite-to-granulite facies zircons: geochronology of the Ivrea Zone (Southern Alps): Contributions to Mineralogy and Petrology, v. 134, p. 380–404.
Wang, K. Y., Li, J. L., and Liu, L. Q., 1991, Petrogenesis of the Fuping grey gneisses: Scientia Geologica Sinica, v. 26, p. 254–267 (in Chinese).
Wang, K. Y., Li, J. L., Hao, J., Li, J. H., and Zhou, S. P., 1996, The Wutaishan mountain belt within the Shanxi Province, Northern China: a record of late Archean collision tectonics: Precambrian Research, v. 78, p. 95–103.
Wilde, S. A., Cawood, P., Wang, K. Y., and Nemchin, A., 1997, The relationship and timing of granitoid evolution with respect to felsic volcanism in the Wutai Complex, North China craton: Proceedings of the 30th International Geological Conference: Precambrian Geology and Metamorphic Petrology, v. 17, p. 75–88.
——— 1998, SHRIMP U–Pb zircon dating of granites and gneisses in the Taihangshan-Wutaishan area: Implications for the timing of crustal growth in the North China craton: The 9th International Conference on Geochronology, Cosmochronology and Isotope Geology, Abstract, Beijing, Chinese Science Bulletin, v. 43, p. 144.
Williams, I. S., and Claesson, S., 1987, Isotopic evidence for the Precambrian Province and Caledonian metamorphism of high grade paragneisses from the Seve Nappes, Scandanavian Caledonides: Contributions to Mineralogy and Petrology, v. 97, p. 205–217.
Wu, C. H., and Zhong, C. T., 1998, The Paleoproterozoic SW–NE collision model for the central North China Craton: Progress of Precambrian Research, v. 21, p. 28–50 (in Chinese).

Wu, J. S., Geng, Y. S., Xu, H. F., Jin, L. G., He, S. Y., and Sun, S. W., 1989, Metamorphic geology of Fuping Group: Journal of Chinese Institute of Geology, v. 19, p. 1–213 (in Chinese).
Wu, J. S., Geng, Y. S., Shen, Q. H., Liu, D. Y., Li, Z. L., and Zhao, D. M., 1991, The early Precambrian significant geological events in the North China Craton: Beijing, Geological Publishing House, p. 1–115 (in Chinese with English abstract).
Wu, C. H., Li, H. M., Zhong, C. T., and Zhuo, Y. C., 2000, TIMS U–PB single zircon ages for the orthogneisses and paragneisses of Fuping Complex: Progress in Precambrian Research, v. 23, p. 130–139 (in Chinese).
York, D., 1969, Least squires fitting of a straight line with correlated errors: Earth and Planetary Science Letters, v. 5, p. 320–324.
Yuan, G. P., and Zhang, R. Y., 1993, The structural environment of the Paleorift in Wutai greenstone belt: Shanxi Geology, v. 8, p. 21–28 (in Chinese).
Zhai, M. G., Guo, J. H., and Yan, Y. H., 1992, Discovery and preliminary study of the Archean high-pressure granulites in North China: Science in China, v. 12, p. 1325–1330.
Zhai, M. G., Guo, J. H., Li, Y. G., and Yan, Y. H., 1995, Discovery of Archean retrograded eclogites in North China and their tectonic implications: Chinese Science Bulletin, v. 40, p. 1590–1594.
Zhai, M. G., Bian, A. G., and Zhai, T. P., 2000, The amalgamation of the supercontinent of North China Craton at the end of Neo-Archean and its break-up during late Paleoproterozoic and Mesoproterozoic: Science in China, v. 43, p. 219–232.
Zhang, Z. Q., Wu, J. S., and Xe, X. J., 1991, REE, Rb-Sr and Sm-Nd ages of the Archean metamorphic rocks of the Lower Fuping Subgroup and their implications: Geochimica, v. 2, p. 118–126 (in Chinese).
Zhao, G. C., 2001, Paleoproterozoic amalgamation of the North China Craton: Geological Magazine, v. 138, p. 87–91.
Zhao, G. C., and Cawood, P. A., 1999, Tectonothermal evolution of the Mayuan assemblage in the Cathaysia Block: implications for Neoproterozoic collision-related assembly of the South China Craton: American Journal of Science, v. 299, p. 309–339.
Zhao, G. C., Wilde, S. A., Cawood, P. A., and Lu, L. Z., 1998, Thermal evolution of Archean basement rocks from the eastern part of the North China craton and its bearing on tectonic setting: International Geology Review, v. 40, p. 706–721.
Zhao, G. C., Cawood, P. A., and Lu, L. Z., 1999, Petrology and P–T history of the Wutai amphibolites: implications for tectonic evolution of the Wutai Complex, China: Precambrian Research, v. 93, p. 181–199.
Zhao, G. C., Wilde, S. A., Cawood, P. A., and Lu, L. Z., 1999a, Thermal evolution of two types of mafic granulites in the North China craton: evidence for both mantle plume and collisional tectonics: Geological Magazine, v. 136, p. 223–240.
——— 1999b, Tectonothermal history of the basement rocks in the western zone of the North China craton and its tectonic implications: Tectonophysics, v. 310, p. 37–53.
——— 2000a, Petrology and P–T path of the Fuping mafic granulites: implications for tectonic evolution of the central zone of the North China Craton: Journal of Metamorphic Geology, v. 18, p. 375–391.
Zhao, G. C., Cawood, P. A., Wilde, S. A., Sun, M., and Lu, L. Z., 2000b, Metamorphism of the basement rocks in the Central Zone of the North China Craton: Implications for Paleoproterozoic evolution: Precambrian Research, v. 103, p. 55–88.
Zhao, G. C., Wilde, S. A., Cawood, P. A., and Sun, M., 2001a, Archean blocks and their boundaries in the North China Craton: Lithological, geochemical, structural and P–T path constraints and tectonic evolution, *in* Cruden, A. R., editor, Precambrian Terrane Boundaries: Precambrian Research, v. 107, p. 45–73.
Zhao, G. C., Cawood, P. A., Wilde, S. A., and Lu, L. Z., 2001b, High-pressure granulite (retrograded eclogites) from the Hengshan Complex, North China Craton: Petrology and tectonic implications, Journal of Petrology, v. 42, 1141–1170.